https://doi.org/10.5194/egusphere-2026-3636
Preprint. Discussion started: 24 July 2026

An Extended Modal Aerosol Dynamics Model (ExMADv1.0) for Simulating Early Nanoparticle Growth

Qihao Lin[1], Jiandong Wang[2,3], Chenxi Li[4], Dian Ding[1,5], Jiaping Wang[1,5], Wei Nie[1,5], Ximeng Qi[1,5], Yuliang Liu[1,5], Xuguang Chi[1,5], and Xin Huang[1,5]

[1]Joint International Research Laboratory of Atmospheric and Earth System Sciences, School of Atmospheric Sciences, Nanjing University, Nanjing 210023, China
[2]State Key Laboratory of Climate System Prediction and Risk Management/Collaborative Innovation Center on Forecast and Evaluation of Meteorological Disasters/China Meteorological Administration Aerosol-Cloud and Precipitation Key Laboratory, Nanjing University of Information Science and Technology, Nanjing 210044, China
[3]School of Atmospheric Physics, Nanjing University of Information Science and Technology, Nanjing 210044, China
[4]School of Environmental Science and Engineering, Shanghai Jiao Tong University, Shanghai 200240, China
[5]National Observation and Research Station for Atmospheric Processes and Environmental Change in Yangtze River Delta, Nanjing 210023, China

Correspondence to: Jiandong Wang (jiandong.wang@nuist.edu.cn)

Abstract. New Particle Formation (NPF) is one of the important sources of aerosol particles in the atmosphere and plays a significant role in global climate change and air quality. Accurately simulating the early growth of nanoparticles from NPF remains critical yet challenging. Specifically, the trimodal framework in current modal schemes often fails to resolve the distinct evolution of nucleation-mode particles and their separation from the background Aitken population. To address this, we developed an Extended Modal Aerosol Dynamics Model (ExMADv1.0) that explicitly incorporates a nucleation mode. This model can be completely driven by observational data for process analysis. The ExMAD model was evaluated against observational data from two representative NPF events in Nanjing, China. A nucleation-resolved decomposition of observed particle size distributions confirms that newly formed particles constitute a distinct sub-25 nm mode during NPF events. Compared with the conventional modal configuration, which captures only ~45% of the observed sub-25 nm particle number concentrations, ExMAD reproduces ~80% of the observed magnitude during the NPF events. ExMAD also reproduces the observed geometric mean diameter (D_g) of the nucleation mode within ~2 nm, a key metric reflecting early-stage growth dynamics. The extended scheme also improves the simulation of particle growth into Cloud Condensation Nuclei (CCN)-relevant size ranges, reducing the overestimation of >50 nm particle concentrations by nearly half relative to the conventional configuration. Sensitivity simulations further show that the Kelvin effect suppresses early-stage condensational growth, delays the transfer of particles from the nucleation mode to larger modes, and limits the uptake of low-volatility organics by the smallest particles. Compared with sectional simulations, the extended modal scheme provides a more realistic representation of sub-25 nm variability while requiring only a ~2.4% runtime increase relative to the default modal configuration, far lower than the cost of sectional schemes. These results demonstrate that the extended scheme offers an

https://doi.org/10.5194/egusphere-2026-3636
Preprint. Discussion started: 24 July 2026

optimal balance between physical realism and computational efficiency, supporting its future application in three-dimensional aerosol-climate simulations.

1 Introduction

Atmospheric aerosols play a pivotal role in the Earth's climate system and pose significant risks to global air quality (Chen et al., 2022; Forster et al., 2020; Fuzzi et al., 2015; Huang et al., 2023; Jia and Quaas, 2023). These impacts are characterized not merely by mass concentration, but significantly by the particle number concentration and size distribution (Fierce et al., 2024; Song et al., 2025; Wu et al., 2022). New particle formation (NPF) serves as a dominant source of particle number at sizes of a few nanometers , thereby significantly altering the aerosol size distribution, particularly within the ultrafine size range (Bousiotis et al., 2021; Deng et al., 2020; Kulmala et al., 2004; Zhang et al., 2012). Through subsequent condensation and coagulation, these newly formed particles grow continuously from a few nanometers to sizes at which they can act as Cloud Condensation Nuclei (CCN). It is estimated that NPF and the subsequent growth contribute approximately 50% of global CCN, playing a critical role in regulating aerosol indirect radiative forcing (Kulmala et al., 2022; Merikanto et al., 2009). Consequently, an accurate representation of these early growth dynamics is essential for climate assessment.

Simulating the complex spatiotemporal evolution of the particle size distribution (PSD) remains a primary challenge in aerosol dynamics modelling. Theoretically, this evolution is governed by the General Dynamic Equation (GDE) consisting of nucleation, condensation, coagulation and transport processes (Li and Cai, 2020; Seinfeld and Pandis, 2016). However, due to the nonlinear integro-differential form of the GDE, obtaining analytical solutions is computationally intractable for realistic atmospheric conditions. To overcome this barrier, three-dimensional models rely on numerical techniques to approximate the PSD. The modal methods are one of the most widely used, representing the PSD as a superposition of lognormal distributions (modes). This treatment offers a balance between computational efficiency and physical realism (Binkowski and Shankar, 1995; Spracklen et al., 2011). Current modal schemes in atmospheric chemistry and climate models, typically adopt a trimodal framework consisting of Aitken, accumulation, and coarse modes (Ackermann et al., 1998; Appel et al., 2017; Binkowski and Roselle, 2003; Lauer et al., 2005; Liu et al., 2012). Advanced frameworks have focused on subdividing the Aitken and accumulation modes to refine the representation of aerosol physicochemical properties (Gao et al., 2017; Kaiser et al., 2014; Liu et al., 2016). However, retaining the Aitken mode as the smallest aerosol subpopulation introduces an intrinsic limitation as the size range of the Aitken mode is one order of magnitude larger than that of newly formed particles with diameters of approximately 1 nm (Cai et al., 2021; Cai and Jiang, 2017; Kürten et al., 2018). This size mismatch makes the trimodal framework less capable of resolving ultrafine particles during the early growth stage.

In contrast to the Aitken-mode aerosol population that largely consists of primary emissions and secondary particles, freshly nucleated particles exhibit distinctly different dynamics characterized by nucleation bursts and intense coagulation scavenging by larger pre-existing aerosols. Their subsequent growth is driven by the condensation of gaseous precursors. Sulfuric acid (SA) is widely identified as the key driver for the initial growth of nanoparticles because of its non-volatile

https://doi.org/10.5194/egusphere-2026-3636
Preprint. Discussion started: 24 July 2026

nature (Deng et al., 2020; Yan et al., 2021; Yao et al., 2018). The oxidation products of volatile organic compounds (VOCs), particularly those with low-volatility, play a dominant role in driving the subsequent growth of these tiny particles to larger sizes (Liu et al., 2024; Tröstl et al., 2016; Zhang et al., 2026). However, these early particle growth dynamics are subject to the Kelvin effect. Due to the high curvature of the particle surface, the equilibrium vapor pressure is elevated, creating a thermodynamic barrier for vapors to condense (Semeniuk and Dastoor, 2020; Wang et al., 2020). Therefore, in the default trimodal framework, treating fresh nuclei within the Aitken mode bypasses the explicit simulation of early growth dynamics, leading to an artificial averaging of particle size and properties. A distinct representation of these particles is thus needed to accurately capture their rapid evolution.

Based on ambient observations, a distinct class of ultrafine particles (< 25 nm in diameter) separated from the Aitken mode has been identified (Mäkelä et al., 1997; Steffen et al., 2005). This independent subpopulation, known as the nucleation mode, acts as a transitional bridge between fresh nuclei and the Aitken mode, explicitly characterizing the dynamics of early nanoparticle growth. To represent this mode, several studies have focused on coupling high-resolution sectional schemes into existing modal frameworks (Bergman et al., 2012; Blichner et al., 2021; Mao et al., 2025). The sectional method discretizes the PSD into bins with flexible size boundaries, making it widely applicable for explicitly resolving ultrafine particle growth (Boy et al., 2006; Cai et al., 2016; Matsui et al., 2011; Zaveri et al., 2008). This strategy improves the representation of ultrafine particle size distributions and CCN-relevant number concentrations. However, this hybrid model framework also introduces a substantial number of aerosol tracers to the model, coming at the expense of high computational demands and numerical diffusion (Riemer et al., 2019; Whitby and McMurry, 1997). Alternately, several global modeling frameworks have incorporated a nucleation mode into modal aerosol representations (McErlich et al., 2025; Tegen et al., 2019; Vignati et al., 2004). While these structural advancements demonstrated the computational efficiency of using a modal approach to track PSD on global scale, they also face certain limitations. Due to simplified chemistry and rigid modal assumptions, existing schemes may not fully resolve the highly non-linear gas-particle partitioning and intermodal microphysics required in three-dimensional atmospheric models.

To address these limitations, we developed a comprehensive modal aerosol model called the Extended Modal Aerosol Dynamics Model (ExMADv1.0), which integrates a dedicated nucleation mode into the existing trimodal framework. Figure 1 provides a schematic overview of how the newly extended modal framework improves upon the traditional trimodal configuration by explicitly resolving the nucleation mode. In the novel framework, the Method of Moments (MOM) serves as the foundation for solving the GDE (Lee et al., 1984; Shen et al., 2020; Yu et al., 2008). The growth kernel in ExMAD accounts for condensational growth by sulfuric acid and organics spanning extremely low to semi-volatility, while incorporating the non-linear Kelvin effect that is neglected in the default trimodal representation. Specifically, we extend the coagulation kernel by using the Gauss-Hermite quadrature to evaluate the double integrals associated with the nucleation, Aitken and accumulation modes. The extended modal structure is validated by our multi-modal fitting analysis of high-resolution particle size distributions from two typical NPF events in Nanjing, China, which identified a distinct nucleation mode separated from the Aitken mode. The model performance was then evaluated against these observational datasets.

https://doi.org/10.5194/egusphere-2026-3636
Preprint. Discussion started: 24 July 2026

Ultimately, this work aims to strike a balance between model efficiency and accuracy, providing robust simulation of aerosol processes in complex atmospheric environments.

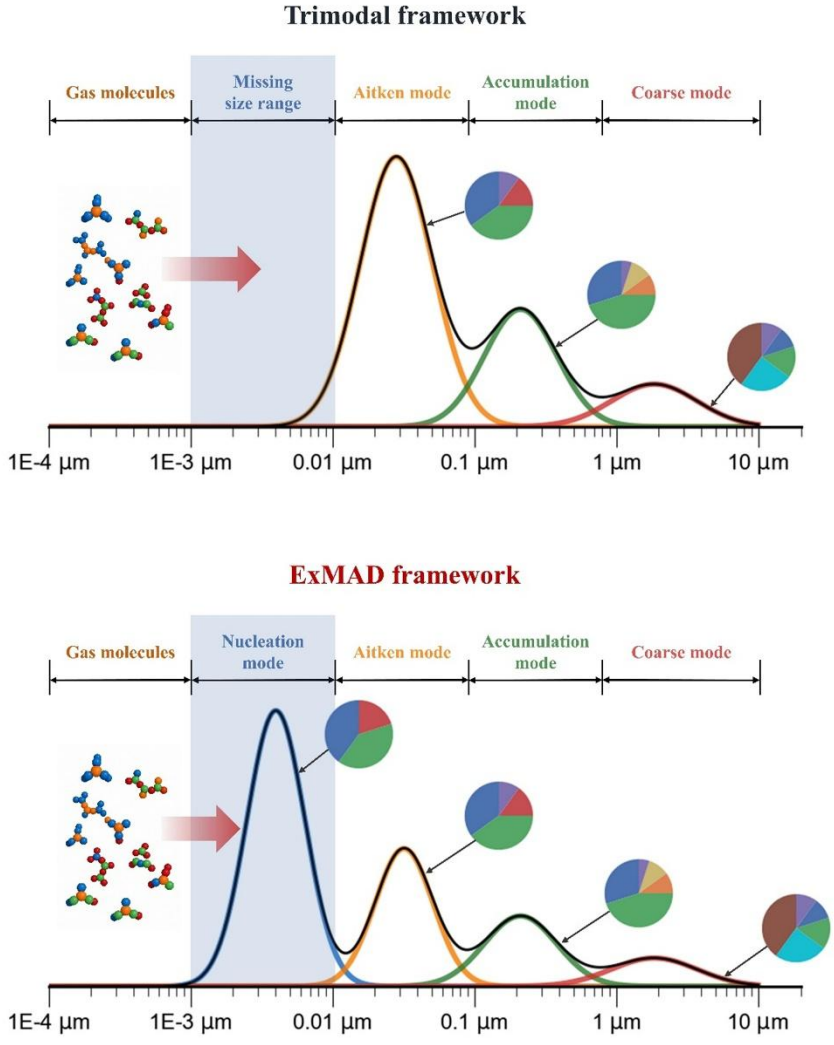

Figure 1. Comparison of the trimodal and ExMAD frameworks for simulating PSD. The ExMAD framework (bottom) explicitly incorporates the nucleation mode (blue curve) to capture NPF and subsequent growth, which is typically unresolved (dashed line) in the standard trimodal framework (top).

2 Methods

2.1 Modal model

This section presents the mathematical formulation of the ExMADv1.0 framework, which is amenable to both observational-data-driven process analysis and integration into three-dimensional atmospheric models. Within this

https://doi.org/10.5194/egusphere-2026-3636
Preprint. Discussion started: 24 July 2026

framework, the PSD is represented as a superposition of lognormal modes that explicitly resolves the nucleation mode. The mathematical formulation is governed by three microphysical processes: (1) new particle formation, which initiates early particle growth by introducing newly formed particles into the nucleation mode; (2) condensational growth driven by sulfuric acid and organic vapors spanning extremely low to semi-volatility, which incorporates an analytical size-dependent Kelvin correction; and (3) coagulation, resolved via a Gauss-Hermite quadrature-based kernel that resolves intra- and inter-modal interactions across the nucleation, Aitken, and accumulation modes. Ultimately, to prevent one mode from growing beyond its size range, a boundary-aware mode-merging scheme with fractional intermodal transfer is specifically applied.

2.1.1 Particle size distribution

In this study, the PSD is formulated as a superposition of three distinct modes (i.e., nucleation, Aitken, and accumulation modes). Each mode is approximated by an independent lognormal distribution, characterized by distinct size ranges and chemical compositions (Bauer et al., 2008; Binkowski and Roselle, 2003; Stier et al., 2005). In this study, the nucleation, Aitken, and accumulation modes are defined over the size ranges of < 25 nm, 25–100 nm, and 100–1000 nm, respectively. Given our primary focus on the dynamics of nanoparticle growth, the coarse mode is excluded from the current simulation. Mathematically, the total PSD is defined as:

$$n(\ln D_p) = \sum_{i=1}^{3} n_i(\ln D_p) = \sum_{i=1}^{3} \frac{N_i}{\sqrt{2\pi} ln\sigma_{gi}} exp\left[-\frac{(lnD_p - lnD_{gi})^2}{2ln^2\sigma_{gi}}\right] \quad (1)$$

where D_p denotes the aerodynamic diameter of particle. $n_i(lnD_p)$ is the PSD of mode i. N_i, D_{gi} and σ_{gi} represent the number concentration, geometric mean diameter, and geometric standard deviation of mode i, respectively.

Instead of directly tracking the geometric parameters, the temporal evolution of the PSD in this framework is achieved through the Method of Moments (MOM). The k-th order moment ($M_{k,i}$) for mode i is defined as the integral of the size distribution weighted by the particle diameter raised to the power of k:

$$M_{k,i} = \int_{-\infty}^{\infty} D_p^k n_i(lnD_p) d(lnD_p) \quad (2)$$

Substituting Eq. (1) into Eq. (2), an explicit analytical relationship between $M_{k,i}$ and the geometric parameters is derived:

$$M_{k,i} = N_i D_{gi}^k exp\left[\frac{k^2}{2} ln^2\sigma_{gi}\right] \quad (3)$$

This equation indicates that the set of three parameters (N_i, D_{gi} and σ_{gi}) can be retrieved by resolving the changes in any three independent moments. In this study, the zeroth ($M_{0,i}$), second ($M_{2,i}$), and third ($M_{3,i}$) moments are adopted to track the temporal evolution of PSD for mode i. While $M_{0,i}$ is strictly equal to the number concentration (N_i), $M_{2,i}$ and $M_{3,i}$ also possess direct physical interpretations, being directly proportional to the total particle surface area and volume, respectively. The diagnostic equations for geometric parameters are presented below:

$$ln^2\sigma_{gi} = \frac{1}{3} ln\left(\frac{M_{0,i}M_{3,i}^2}{M_{2,i}^3}\right) \quad (4)$$

https://doi.org/10.5194/egusphere-2026-3636
Preprint. Discussion started: 24 July 2026

$$D_{gi} = \left(\frac{M_{2,i}}{M_{0,i}}\right)^{\frac{3}{2}} \left(\frac{M_{3,i}}{M_{0,i}}\right)^{-\frac{2}{3}} \quad (5)$$

As detailed in previous theoretical frameworks (Whitby and McMurry, 1997; Yu and Lin, 2010), the GDE is converted into a system of moment-based ordinary differential equations, serving as the core dynamic framework of this study. The temporal evolution of the k-th moment for mode i is governed by:

$$\frac{\partial M_{k,i}}{\partial t} = \frac{\partial M_{k,i}}{\partial t}\Big|_{\text{npf}} + \frac{\partial M_{k,i}}{\partial t}\Big|_{\text{cond}} + \frac{\partial M_{k,i}}{\partial t}\Big|_{\text{coag}} \quad (6)$$

where the terms on the right-hand side represent the rates of change in the k-th moment driven by new particle formation, condensation, and coagulation, respectively, which will be detailed in the following sections.

2.1.2 New particle formation

Implementing an aerosol scheme requires defining an initial injection size for simulating particle growth. While small initial sizes (< 3 nm) better capture early growth, they suffer from high uncertainties in survival probability (Kulmala et al., 2017). Conversely, an excessively large initial diameter can lead to the neglect of self-coagulation and an overestimation of particle formation rates (Blichner et al., 2021; Olenius and Riipinen, 2017). In this study, we utilize a particle formation rate calculated at 4 nm, aligning with the lower detection limit of our observational instruments (detailed in Sect. 2.2). This 4 nm threshold maintains robust model stability and falls well within the typical range of initial diameters (1–10 nm) suggested by previous studies (Chen et al., 2021; Jacquot and Sartelet, 2025; Lee et al., 2013; Yu and Luo, 2009). The newly formed particles are thus introduced into the nucleation mode following a lognormal distribution with a geometric mean diameter of 4 nm, formulated as:

$$\frac{\partial M_{k,Nuc}}{\partial t}\Big|_{\text{npf}} = J_{D_p^*} D_p^* \exp\left[\frac{k^2}{2} ln^2 \sigma_g^*\right] \quad (7)$$

where $M_{k,Nuc}$ denotes the k-th moment in the nucleation mode. D_p^* and $J_{D_p^*}$ are the initial diameter and particle formation rate at the initial diameter, respectively. σ_g^* , denoting the geometric standard deviation of the assumed initial size distribution, is set to 1.5 in this study (Deng et al., 2022).

The formation rate at D_p^* was calculated using the formulation given in previous studies (Dal Maso et al., 2005; Kulmala et al., 2012; Westervelt et al., 2013):

$$J_{D_p^*} = \frac{dN_{[D_p^*, D_{pu})}}{dt} + F_{Coag} + F_{Cond} \quad (8)$$

where D_{pu} is the upper bound of particle size in the nucleation mode. $N_{[D_p^*, D_{pu})}$ denotes the number concentration in the size range from D_p^* to D_{pu}. F_{Coag} represents particle loss due to self-coagulation and coagulation scavenging. F_{Cond} accounts for particle growth beyond D_{pu} due to condensation. This term is neglected here because particles rarely grow out of the nucleation mode before formation ceases. Since this study focuses on the early growth of secondary particles, primary emission is not included in the current version of the model.

https://doi.org/10.5194/egusphere-2026-3636
Preprint. Discussion started: 24 July 2026

2.1.3 Condensation kernel

To rigorously quantify the growth of nucleation-mode particles, ExMAD calculates the condensation of both sulfuric acid (SA) and oxygenated organic molecules (OOMs), generated from the atmospheric oxidation of precursor VOCs. Furthermore, we explicitly incorporate the size-dependent Kelvin effect into the growth kernel, a mechanism neglected in standard modal schemes (Binkowski and Shankar, 1995; Semeniuk and Dastoor, 2020). While SA is treated as a discrete species, the OOMs are categorized into surrogate volatility bins based on the Volatility Basis Set (VBS) mechanism (Donahue et al., 2011; Shrivastava et al., 2011; Zhao et al., 2024). The organic species span from extremely low volatility (ELVOCs) to semi-volatility (SVOCs), establishing both their thermodynamic phase-partitioning and distinct kinetic mass-transfer properties.

To accurately simulate how these vapors interact with the aerosol population, an explicit size-resolved treatment is indispensable for capturing the Kelvin barrier, which thermodynamically restricts the condensation of volatile species onto nanoparticles (Patoulias and Pandis, 2022; Tang et al., 2025; Zhang et al., 2012). Given that this curvature effect is highly non-linear and disproportionately suppresses the growth of nucleation-mode particles, traditional explicit integration over the entire modal spectrum becomes mathematically cumbersome. By introducing an analytical approximation of the modal-average Kelvin term and coupling it with the VBS mechanism, our model effectively simulates the volatility- and size-dependent condensational growth. Overall, the net change of the k-th moment due to multi-component condensation is formulated as:

$$\left.\frac{\partial M_{k,i}}{\partial t}\right|_{cond} = \sum_c \Psi_{k,i,c}\left(C_{gas,c} - \overline{C_{eq,i,c}}\right) \tag{9}$$

$$\overline{C_{eq,i,c}} = C_{sat,c}(T) \cdot \chi_{i,c} \cdot \overline{KE_{i,c}} \tag{10}$$

where $\Psi_{k,i,c}$ is the moment transfer coefficient, which governs the kinetic diffusion of condensable species c onto the k-th moment of mode i. $C_{gas,c}$ and $\overline{C_{eq,i,c}}$ represent the ambient gas-phase concentration and the equivalent surface equilibrium concentration of species c. $C_{sat,c}(T)$ is the saturation vapor concentration of species c over a flat surface at a specific temperature T. $\chi_{i,c}$ is the mole fraction in the particle phase. $\overline{KE_{i,c}}$ denotes the modal-average Kelvin effect factor for species c in mode i. Rather than a simple geometric mean, this factor is defined as the average of the size-dependent curvature effect weighted by the moment mass transfer coefficient across the modal size distribution. Detailed mathematical formulations and explicit expressions for both $\Psi_{k,i,c}$ and $\overline{KE_{i,c}}$ are provided in the Section S1 in the Supplement.

2.1.4 Coagulation kernel

To accurately quantify coagulation, which scales quadratically with number concentration, we developed a comprehensive coagulation kernel that extends the established bimodal parameterizations (Whitby and McMurry, 1997) to a trimodal framework. This scheme explicitly calculates the mass-conserving interactions within and between the nucleation, Aitken, and accumulation modes. The kernel resolves two distinct processes. First, it captures intramodal coagulation (self-

https://doi.org/10.5194/egusphere-2026-3636
Preprint. Discussion started: 24 July 2026

coagulation), where collisions between particles of similar sizes serve as an alternative growth pathway for nucleation-mode particles alongside condensation (Stolzenburg et al., 2005). Second, it accounts for intermodal coagulation, acting as a coagulation sink whereby smaller nucleation-mode particles are scavenged by larger pre-existing populations in the Aitken and accumulation modes (Cai et al., 2018; Kerminen et al., 2018). Accordingly, the net change in the k-th moment for mode i can be formulated as:

$$\left.\frac{\partial M_{k,i}}{\partial t}\right|_{\text{coag}} = R_{\text{self,i}} - \sum_{\text{j>i}} R_{\text{i}\to\text{j}}^{\text{sink}} + \sum_{j<i} R_{\text{j}\to\text{i}}^{\text{gain}} \tag{11}$$

where $R_{self,i}$ represents the rate of change due to intramodal coagulation. The second term describes the coagulation sink, where mode i is scavenged by all larger modes j. The third term represents the intermodal accretion, accounting for the transfer of moments to mode i from the coagulation of smaller modes j. The detailed expanded formulations for each term corresponding to the nucleation, Aitken, and accumulation modes are provided in Section S2. Each of these terms contains complex double integrals that make analytical closed-form solutions difficult to obtain. To address this, we adopt a Gauss-Hermite quadrature-based moment treatment, which efficiently transforms these continuous integrals into discrete double summations over the quadrature nodes (Fierce et al., 2021; McGraw, 1997; McGraw and Wright, 2003; Wright et al., 2001).

The approximation of $R_{self,i}$ can be expressed as:

$$R_{self,i} \approx \frac{N_i^2}{\pi}\sum_{l=1}^{N_{node}}\sum_{q=1}^{N_{node}}\left[\frac{1}{2}\left(D_{p,l}^3 + D_{p,q}^3\right)^{k/3} - D_{p,l}^k\right]\beta\left(D_{p,l}, D_{p,q}\right)\omega_l\omega_q \tag{12}$$

$$D_{p,l(q)} = D_{gi}\exp(\sqrt{2}x_{l(q)}ln\sigma_{gi}) \tag{13}$$

where N_i is the number concentration of mode i. N_{node} denotes the number of quadrature nodes. The indices l and q denote the quadrature nodes corresponding to the two colliding particles. $D_{p,l}$ and $D_{p,q}$ are both derived from the standard Gauss-Hermite abscissas (x_l and x_q) through the coordinate transformation governed by the distribution parameters of mode i. $\beta\left(D_{p,l}, D_{p,q}\right)$ denotes the collision frequency between two particles.

The calculation of intermodal coagulation differs from that of intramodal coagulation, since the colliding particles originate from two distinct populations (mode i and mode j). The double integral is approximated using two independent sets of quadrature nodes. The second and the third term in Eq. (11) are approximated by:

$$R_{i\to j}^{sink} \approx \frac{N_i N_j}{\pi}\sum_{l=1}^{N_{node}}\sum_{q=1}^{N_{node}} D_{p,l}^k\,\beta\left(D_{p,l}, D_{p,q}\right)\omega_l\omega_q \tag{14}$$

$$R_{j\to i}^{gain} \approx \frac{N_i N_j}{\pi}\sum_{l=1}^{N_{node}}\sum_{q=1}^{N_{node}}\left[\left(D_{p,l}^3 + D_{p,q}^3\right)^{k/3} - D_{p,l}^k\right]\beta\left(D_{p,l}, D_{p,q}\right)\omega_l\omega_q \tag{15}$$

where the subscripts l and q here denote the l-th node of mode i and the q-th node of mode j, respectively. $D_{p,l}$ and $D_{p,q}$ are transformed from the standard quadrature nodes using the PSD parameters of the mode i and mode j, respectively. The approximations efficiently resolve the complex integro-differential coagulation equations while strictly preserving mass conservation.

https://doi.org/10.5194/egusphere-2026-3636
Preprint. Discussion started: 24 July 2026

2.1.5 Mode merging

To prevent artificial overlap among adjacent modes during particle growth, we apply a boundary-aware mode-merging treatment after condensation. In the present trimodal configuration, cut-off diameters are set at 25 nm and 100 nm to distinguish the nucleation, Aitken, and accumulation modes. The two thresholds control intermodal transfer from the nucleation mode to the Aitken mode and from the Aitken mode to the accumulation mode.

However, the significant size overlap between the nucleation and Aitken modes makes abrupt intermodal transitions problematic, inducing severe numerical instabilities and non-physical distribution distortions (Weisenstein et al., 2007). To achieve a smooth transition, we adopt a fractional transfer mechanism inspired by Liu et al. (2016), who evaluated aerosol evolution through the accumulation of molecular monolayers. Specifically, the original theoretical transfer fraction is multiplied by a smoothing factor, which scales the intermodal transfer based on the ratio of the condensed monolayers in a given time step to the target monolayers needed to reach the cut-off diameter. The actual transfer fraction (ΔF) for the number and mass concentrations is determined by the following expressions:

$$\Delta F = \Delta F' \left[1 - \exp\left(-\frac{\Delta N_{Layer}}{N_{Target}}\right)\right] \quad (16)$$

$$\Delta N_{Layer} = \frac{GR \cdot \Delta t}{\overline{D_c}} \quad (17)$$

$$N_{Target} = \frac{D_{cut} - D_g}{2 \cdot \overline{D_c}} \quad (18)$$

where $\Delta F'$ represents the theoretical fraction of the log-normal distribution tail exceeding the cut-off diameter (D_{cut}). ΔN_{Layer} represents the number of molecular monolayers condensed within a time interval, which is determined by the geometric mean growth rate (GR), the time interval (Δt), and the equivalent thickness of a single condensed monolayer ($\overline{D_c}$). N_{Target} represents the target number of molecular monolayers required to reach D_{cut}. Generally, the bracketed term in Eq. (16) serves as a scaling factor based on the mode's proximity to the boundary. It approaches unity when D_g is close to D_{cut}, while suppressing the transfer fraction at larger distances to facilitate a smooth moment transfer.

2.2 Field campaign and instruments

The observational data used in this study were collected from ground-based measurements conducted from 1 August to 31 August 2019 at the Station for Observing Regional Processes of the Earth System (SORPES). This station is located in the Xianlin campus of Nanjing University, northeast of downtown Nanjing (118°57′E, 32°07′N). It is influenced by air masses from both North China Plain and the sub-tropical forest region, making it an excellent location for studying atmospheric processes (Ding et al., 2016, 2013).

To constrain the model simulation, gaseous precursors were measured with high time resolution. SA and oxygenated organic molecules (OOMs) were measured by a chemical ionization atmospheric pressure interface time-of-flight mass spectrometer with nitrate reagent ions (nitrate CI-APi-TOF; Aerodyne Research Inc. and Tofwerk AG) (Jokinen et al., 2014;

https://doi.org/10.5194/egusphere-2026-3636
Preprint. Discussion started: 24 July 2026

Liu et al., 2023). Binned positive matrix factorization (binPMF) was introduced to identify and separate peaks in the complex mass spectral data (Zhang et al., 2019). Subsequent categorization of the OOMs into different groups such as aliphatics, aromatics, isoprene, and monoterpenes was performed based on the oxidation pathways of their precursor VOCs and the binPMF results as described in previous works (Liu et al., 2021; Nie et al., 2022).

Particle size distribution (PSD) data provided the reference dataset for assessing the model simulations. The PSD with a size range from 4 nm to 1000 nm was collected by two Scanning Mobility Particle Sizers (SMPS, TSI Inc.) and an Aerodynamic Particle Sizer (APS, TSI Inc.) (Chen et al., 2023; Qi et al., 2024). The two sets of SMPS, equipped with a long DMA (Model 3088) and a nano-DMA (Model 3085), measured the PSD ranging from 4 nm to 500 nm. Then the APS extended the measurement capability of particle size to more than 500 nm, ensuring continuous characterization of particles from the nucleation mode through the accumulation mode.

Based on the observational dataset, two distinct NPF episodes, namely, Event 1 and Event 2, were selected for detailed simulation and analysis. The events occurred on August 18 and 16, 2019, respectively. The observed precursor concentrations and meteorological parameters from these days were used as time-dependent inputs to drive the model, while the measured PSD evolution was used to evaluate the simulation results.

2.3 Model configurations and scenarios

The zero-dimensional box model was configured to simulate the temporal evolution of particle size distributions during NPF events. For each selected event, the simulation duration was set to 10 hours, covering the complete NPF process from the initial nucleation burst to the subsequent particle growth. We employ an operator splitting approach in our model to solve the aerosol dynamics equation, which separates the inherently coupled processes into several sub-processes for individual solution. The operator splitting interval is 300 seconds, balancing both computational efficiency and model accuracy (Li et al., 2023; Lin et al., 2024). Consequently, all input data, including gas-phase precursors and meteorological parameters, were interpolated to this 300-s interval to synchronously drive the model. To quantify the contribution of different organic vapors to particle growth, the measured OOMs were categorized into 9 surrogate species based on their volatility (Liu et al., 2021; Nie et al., 2022). These volatility bins span a saturation concentration (c^*) range from 10^{-8} to 1 μg m^{-3}, separated by one order of magnitude.

Prior to the simulations, the observed PSDs were decomposed into modal components using a Gaussian Mixture Model (see Section S3 in the Supplement). This decomposition was used not only to derive the initial modal parameters, but also to diagnose whether the observed sub-100 nm particle population could be adequately represented without explicitly separating freshly formed particles from the background Aitken mode.

Four distinct simulation scenarios were designed to investigate the impacts of modal representation of aerosol dynamics. The Base scenario corresponds to a conventional modal representation in which the sub-100 nm population is not explicitly separated into nucleation and Aitken modes. The ExtMod scenario corresponds to the configuration of ExMAD in which the nucleation mode is resolved in addition to the Aitken and accumulation modes. The comparison between Base and ExtMod

https://doi.org/10.5194/egusphere-2026-3636
Preprint. Discussion started: 24 July 2026

was therefore designed to isolate the impact of explicitly resolving the nucleation mode, as suggested by the decomposition of the observed PSD.

Except for the investigation of modal structure, we further designed two specific scenarios to discuss the impact of specific physical mechanisms and the computational efficiency and accuracy of different models. The KelOff scenario adopts the same modal configurations as the ExtMod scenario but without the Kelvin effect during condensational growth. It is designed to quantify the influence of the Kelvin effect on the aerosol dynamics, especially the growth of nucleation mode particles. The Sec scenario is employed to validate the numerical performance of the modal approaches. A sectional model was applied over the size range of 4–1000 nm, with different resolutions of 20, 50, and 100 bins (denoted as Sec20, Sec50, and Sec100, respectively).

Finally, the model performance was quantitatively assessed using three statistical indicators: Normalized Mean Bias (NMB), Normalized Mean Error (NME), and Root Mean Square Error (RMSE). These metrics were calculated to compare the simulated particle number concentrations and PSD against the observed data, enabling a robust evaluation of the accuracy of different scenarios. The detailed mathematical definitions of these indicators are presented in Section S4 in the Supplement.

3 Results and discussion

3.1 Nucleation-Resolved Decomposition of Observed PSD

The temporal evolution of observed PSD during Event 1 is presented in Figure 2a, exhibiting a distinct and continuous particle growth pattern. Specifically, a sharp increase in the number concentration of nucleation-mode particles (D_p < 25 nm) started from 9:30 a.m. and lasted for approximately 6 hours, followed by a continuous growth into the Aitken mode over the subsequent hours. The high number concentration of sub-25 nm particles suggests a strong growth rate of newly formed particles, while the continuous increase of particle size reflects the condensation of vapors onto these particles.

This observed evolution suggests that more than one mode is necessary to resolve the newly formed particles from the background particles in the sub-100 nm population throughout the event. To examine this issue, we compared a conventional bimodal decomposition (Figure 2b) with a nucleation-resolved three-mode decomposition (Figure 2c). The bimodal fit uses a D_g cutoff of 100 nm to distinguish Aitken from accumulation modes. It tends to merge the freshly nucleated particles into the background Aitken mode, resulting in a blurred distribution. In contrast, the nucleation-resolved decomposition resolves this limitation by splitting the sub-100 nm population into distinct nucleation and Aitken modes, separated by a size threshold of approximately 25 nm. This refinement successfully isolates the newly formed particles from the larger background aerosol, allowing the fitted curve to faithfully trace the entire particle growth process. The corresponding comparison between the conventional bimodal representation and the nucleation-resolved decomposition for Event 2 is

https://doi.org/10.5194/egusphere-2026-3636
Preprint. Discussion started: 24 July 2026

provided in Fig. S1. The latter better captures the observed separation and subsequent growth of the newly formed particle population.

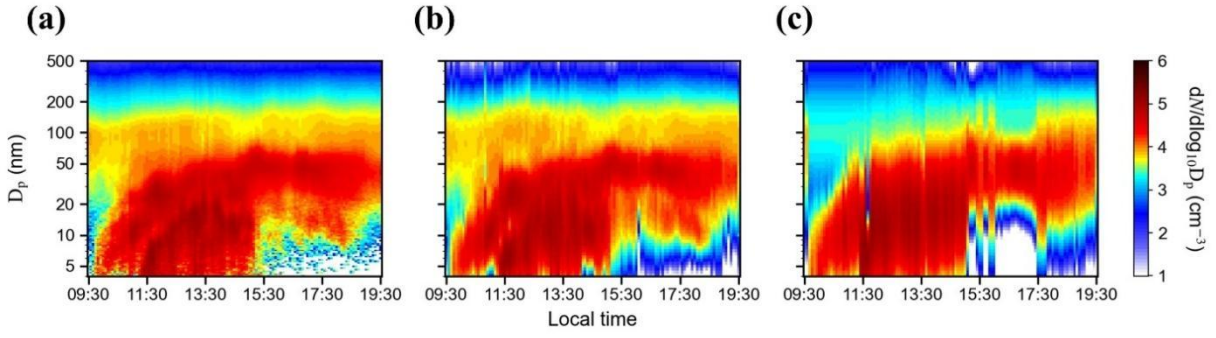

Figure 2. Temporal evolution of PSD during Event 1. (a) The observed PSD. (b) Reconstructed PSD based on the conventional bimodal decomposition. (c) Reconstructed PSD based on the nucleation-resolved three-mode decomposition. The color bar shows the log scale of PSD.

To further quantify the discrepancies between the two fitting approaches, we calculated the time-averaged PSD over the entire duration of the NPF event. Figure 3 presents the scatter-plot comparison between the observed and fitted PSDs for Event 1. The nucleation-resolved decomposition (magenta circles) exhibits a high degree of consistency with the observations, with data points closely distributed around the 1:1 line across the entire size spectrum. In contrast, the bimodal fit (green circles) shows pronounced deviations, particularly in the high-concentration range. Statistically, this discrepancy is clearly reflected in the performance metrics. As detailed in Table S2, for Event 1, the three-mode decomposition yields a substantial improvement over the two-mode fitting, reducing the normalized mean error (NME) from 0.10 to 0.04, the normalized mean bias (NMB) from -0.03 to -0.02, and the root mean square error (RMSE) from 1070.0 to 550.4, compared to the two-mode composition.

This comparison demonstrates that the observed PSD evolution during NPF cannot be represented adequately without explicitly separating the nucleation mode from the background Aitken population. Neglecting this mode leads to a systematic distortion of the PSD shape and a misinterpretation of the particle growth kinetics. This observational finding provides a strong physical justification for our model scenario design in Sect. 2.3. The ExtMod scenario adopts the nucleation-resolved modal structure to capture the detailed NPF process, while the Base scenario is configured to quantify the discrepancies in simulated aerosol properties arising from these two modal representations.

https://doi.org/10.5194/egusphere-2026-3636
Preprint. Discussion started: 24 July 2026

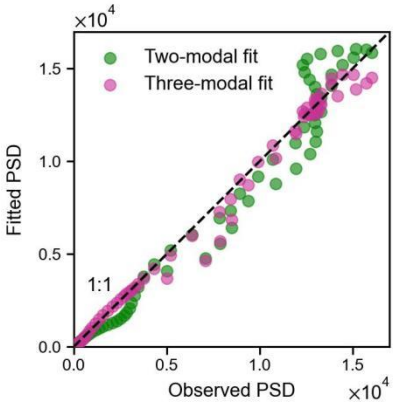

Figure 3. Scatter plot of PSD reconstructed from the two decomposition schemes as a function of the observed PSD for Event 1. The PSDs are time-averaged over the entire NPF period. The bimodal decomposition results are represented by green circles, and the nucleation-resolved decomposition results are shown as magenta circles. The black dashed line indicates the 1:1 reference line.

The modal parameters derived from the nucleation-resolved decomposition are summarized in Table 1. The parameters are averaged over the entire event. For both NPF events, the time-averaged number concentrations for the nucleation and Aitken modes consistently reached the order of 10^4 cm^{-3}, highlighting the dominance of newly formed particles and their subsequent growth. Specifically, the D_g for the nucleation mode were averaged at 12.9 nm and 13.3 nm for Event 1 and Event 2, respectively, whereas the Aitken mode exhibited larger D_g values of 37.9 nm and 41.4 nm, showing a clear modal separation. These fitted characteristics, particularly the distinct modal separation and the magnitude of number concentrations, align well with previous studies (Deng et al., 2022; Qi et al., 2015). The consistency of the nucleation-resolved decomposition with the observations indicates that these modal parameters provide an observationally constrained description of the evolving nucleation, Aitken, and accumulation populations. Therefore, in the following Sect. 3.2, we will utilize these observationally constrained modal characteristics as the benchmark for evaluating the simulation performance.

Table 1. Summary of the time-averaged modal parameters derived from the nucleation-resolved decomposition for Event 1 and Event 2. The parameters include number concentration (N), geometric mean diameter (D_g), and geometric standard deviation (σ_g) for nucleation, Aitken and accumulation modes.

	Event 1			Event 2		
	$N\ (cm^{-3})$	$D_g\ (nm)$	σ_g	$N\ (cm^{-3})$	$D_g\ (nm)$	σ_g
Nucleation mode	2.2×10^4	12.9	1.6	1.1×10^4	13.3	1.5
Aitken mode	1.2×10^4	37.9	1.5	1.6×10^4	41.4	1.4
Accumulation mode	3.4×10^3	104.9	1.7	3.8×10^3	124.3	1.8

https://doi.org/10.5194/egusphere-2026-3636
Preprint. Discussion started: 24 July 2026

3.2 Model evaluation

3.2.1 Evaluation of Particle Number and Size Evolution

Building on the evidence for explicit nucleation-mode separation established in Sect. 3.1, this section quantitatively evaluates the influence of different modal representations on the aerosol dynamics and simulated PSD evolution. Figure 4 presents a comprehensive comparison of the observed growth trajectory of particles and their representations in the Base and ExtMod scenarios for the two selected NPF events. The top row (Figure 4a and Figure 4b) displays the observed PSDs for Event 1 and Event 2, respectively. The middle row (Figure 4c and Figure 4d) illustrates the simulation results from the Base scenario, which adopts the modal structure of the Aitken and accumulation modes. The bottom row (Figure 4e and Figure 4f) depicts the results from the ExtMod scenario, which incorporates the explicit nucleation mode.

In the Base scenario, freshly formed particles are directly merged into the Aitken mode, causing the simulated size distribution of ultrafine particles to appear overly smooth and broadened. This treatment obscures the observed separation between the newly formed ultrafine particles and the pre-existing background population, particularly during the early growth stage, and artificially accelerates the shift of the PSD toward larger diameters. In contrast, the ExtMod scenario provides a much clearer and more physically realistic representation of the ultrafine aerosol population. By preserving the independent distribution and dynamics of these particles, the ExMAD model faithfully captures the time-dependent trajectory of the sub-25 nm population growth into the Aitken size range, thereby more closely reproducing the observed PSD structure in both events.

To further substantiate the structural differences in the PSD evolution shown in Figure 4, we quantified the model performance using size-integrated particle number metrics. Because the Base scenario does not explicitly resolve the nucleation mode, N_{4-25} (particle number concentration in the 4–25 nm range) was used as a common size-integrated metric to compare the two model configurations in representing ultrafine particles. As illustrated in Figure 5a and Figure 5b, the Base scenario exhibits a significant discrepancy, reproducing only about 40% of the observed magnitude in both events. In contrast, ExtMod successfully captures the temporal evolution of N_{4-25}, with event-averaged concentrations reaching approximately 77% and 85% of the observations for Event 1 and Event 2, respectively. For Event 1, ExtMod improves the NME from 0.54 to 0.27, the NMB from -0.54 to -0.23, and the RMSE from 1.61×10^4 to 7.81×10^3 relative to the Base scenario, confirming that an explicit nucleation-mode representation is essential for reproducing the abundance of newly formed particles. A similar improvement is also found for Event 2, for which ExtMod consistently outperforms the Base scenario across three evaluation metrics. The detailed metrics of model evaluation for both events are provided in Table S3 in the Supplement. Note that nucleation mode particles exhibit very short atmospheric lifetimes, typically on the order of minutes to a few hours. Their concentrations therefore decay rapidly with distance from the source region, implying that N_{4-25} is influenced primarily by local formation and growth processes rather than by regional transport (Dai et al., 2017; Kerminen et al., 2018). Consequently, the better performance of ExtMod indicates that our model substantially improves the simulation of the ultrafine-particle dynamics.

https://doi.org/10.5194/egusphere-2026-3636
Preprint. Discussion started: 24 July 2026

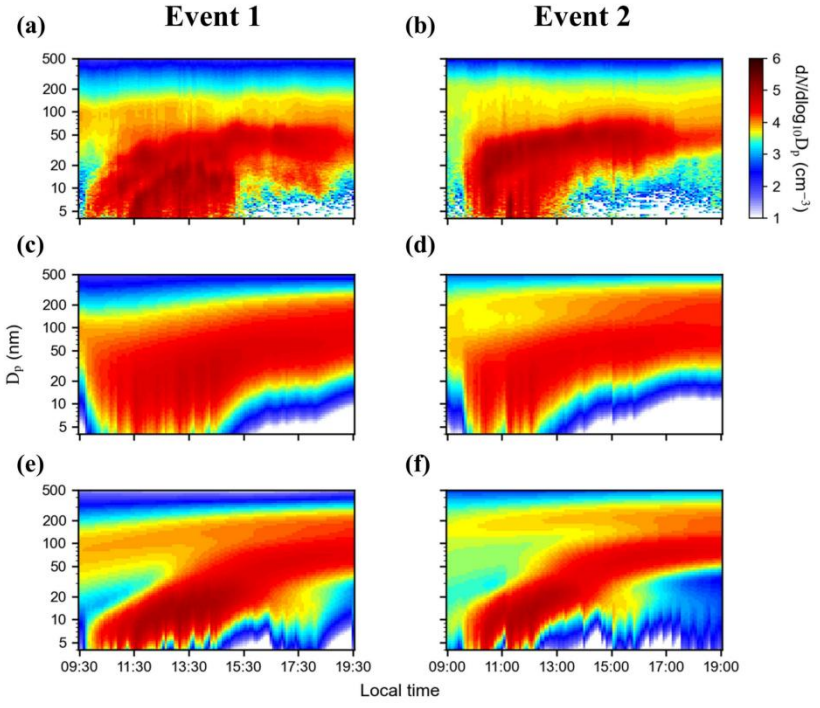

Figure 4. Comparison of the temporal evolution of PSD between observations and box model simulations for Event 1 (left panels) and Event 2 (right panels). (a, b) The observed PSD. (c, d) The simulated PSD for the Base scenario. (e, f) The simulated PSD for the ExtMod scenario. The color bar shows the log scale of PSD.

The particle number concentration in the 25–100 nm size range (N_{25-100}) was then used to evaluate model performance during the stage where newly formed particles grow into the Aitken size range. For Event 1, the Base scenario exhibits a moderate positive bias in N_{25-100}, whereas ExtMod exhibits a moderate negative bias (Figure 5c). According to Table S4 in the Supplement, the Base scenario yields an NME of 0.26 and an NMB of 0.23, while ExtMod produces an NME of 0.29 and an NMB of -0.19. This indicates that, for this event, ExtMod shifts the bias in N_{25-100} from overestimation to underestimation but does not significantly reduce the overall error. For Event 2, the contrast between the two scenarios becomes more pronounced, with ExtMod showing a stronger low bias (Figure 5d). However, the apparently better performance of the Base scenario in Event 2 likely reflects error compensation rather than a more faithful representation of particle growth into the Aitken size range. Notably, our current model focuses mainly on gas-particle partitioning and coagulation dynamics. The direct contribution from primary emissions, which can account for more than 50% of the Aitken mode particle number concentration in urban environments (Cai et al., 2020; Chen et al., 2018; Zhang et al., 2022), is omitted from these simulations. Moreover, unlike the short-lived nucleation mode, Aitken-mode particles have substantially longer atmospheric lifetimes and are therefore more heavily influenced by regional transport and primary emission sources (Seinfeld and Pandis, 2016; Williams et al., 2002). Therefore, N_{25-100} constitutes a more stringent metric than N_{4-25}, and the model performance in this size range mainly highlights the missing effects of primary emissions and transport rather than invalidating the structural advantage of the nucleation-resolved modal representation. Further efforts will focus on

https://doi.org/10.5194/egusphere-2026-3636
Preprint. Discussion started: 24 July 2026

addressing this limitation by integrating number concentration emission inventories and extending the current framework to three-dimensional atmospheric chemical transport models.

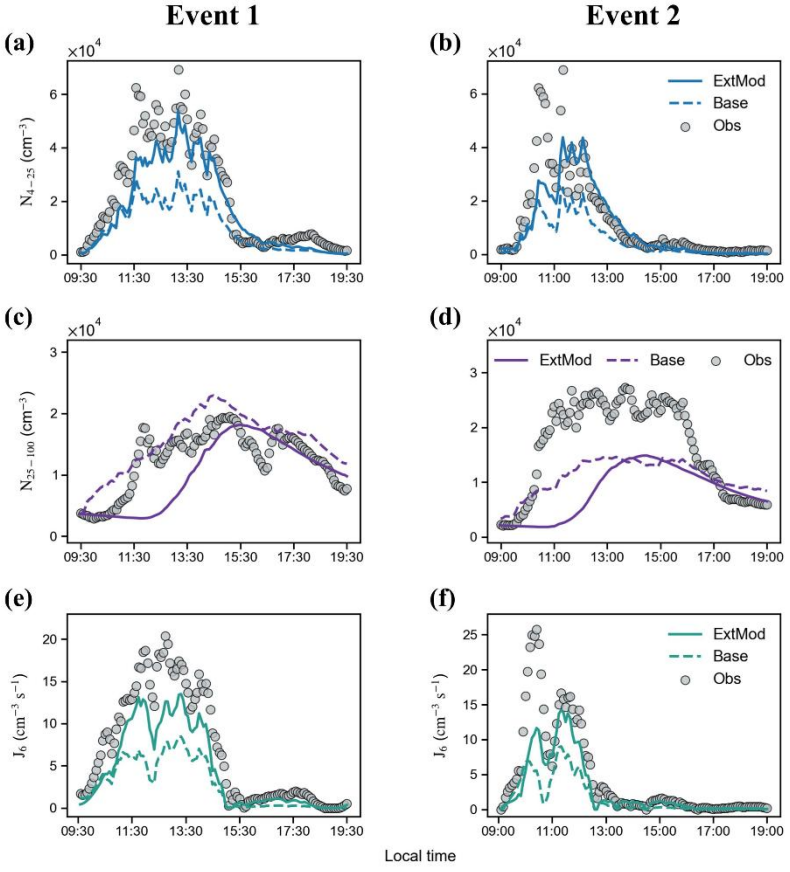

Figure 5. Comparison of the temporal evolution of observed and simulated parameters for Event 1 (left panels) and Event 2 (right panels). (a, b) The number concentration of particles in the sub-25 nm size range. (c, d) The number concentration of particles in the 25-100 nm size range. The solid line, dashed line and scatter plots represent particle number concentration for the Base scenario, ExtMod scenario and field observation, respectively. (e, f) The particle formation rate at 6 nm.

The particle formation rate at 6 nm (J_6) was further examined as an additional diagnostic of the model ability to represent the appearance and early survival of newly formed particles. As shown in Figure 5e and Figure 5f, both events exhibit the same pattern. ExtMod consistently predicts higher J_6 values than the Base scenario and more closely tracks the temporal evolution of the observations. The event-averaged J_6 calculated from the observed PSD are 6.8 cm^{-3} s^{-1} and 4.5 cm^{-3} s^{-1} for Event 1 and Event 2, respectively. For Event 1, the event-averaged simulated J_6 increases from 2.7 cm^{-3} s^{-1} in the Base scenario to 4.5 cm^{-3} s^{-1} in ExtMod, demonstrating a substantially improved representation of particle formation at 6 nm. A similar improvement is found for Event 2, for which the event-averaged simulated J_6 increases from 1.6 cm^{-3} s^{-1} in the Base scenario to 2.8 cm^{-3} s^{-1} in ExtMod. These results indicate that explicitly resolving the nucleation mode improves not only the simulated abundance of ultrafine particles but also their effective survival and growth into the 6 nm size range. However, the

https://doi.org/10.5194/egusphere-2026-3636
Preprint. Discussion started: 24 July 2026

simulated J_6 still underestimates the observed level, suggesting that uncertainties in precursor supply and initial growth processes may still limit the model performance (Gierens et al., 2014; Korhonen et al., 2011; Young et al., 2013). Overall, the J_6 comparison, coupled with the improvements in PSD structure and N_{4-25}, further confirms that the nucleation-resolved modal framework outperforms the conventional configuration in representing early nanoparticle formation and growth.

3.2.2 Particle Growth and CCN activation potential

Having evaluated the performance of ExtMod in reproducing particle number concentrations, we further examine whether the model can capture the size growth of newly formed particles, as represented by the geometric mean diameter (D_g). It serves as a critical microphysical parameter that reflects the dynamic competition between the nucleation of new particles (which tends to decrease the mean size) and the subsequent condensation growth and coagulation, which shift the population toward larger diameters. Figure 6 compares the temporal evolution of D_g derived from the nucleation-resolved decomposition in Sect. 3.1 with that simulated by ExtMod. For the nucleation mode (Figure 6a and Figure 6b), ExtMod closely tracks the observed D_g evolution and captures the growth of freshly formed particles within the 10–20 nm size range. The event-averaged simulated D_g of the nucleation mode is 14.4 nm for Event 1 and 15.1 nm for Event 2, showing a slight bias relative to the decomposition-derived observational values of 12.9 and 13.3 nm, respectively.

For the Aitken mode (Figure 6c and Figure 6d), ExtMod captures the general temporal variability in D_g, including the influence of particles transferred from the nucleation mode, but it systematically overestimates the modal mean size. The event-averaged simulated Aitken-mode D_g reaches 56.8 nm for Event 1 and 59.4 nm for Event 2, compared with the observational values of 37.9 and 41.4 nm, respectively. In addition to this positive size bias, a temporal mismatch is also evident in the simulated Aitken-mode evolution. Specifically, the observed Aitken-mode D_g typically decreases shortly after the onset of the event, whereas the simulated minimum occurs later, indicating a delayed response of the modal transfer process. This mismatch is likely related to the simplified representation of intermodal transfer in the modal framework, which compresses the continuous growth of particles across the nucleation–Aitken boundary into a discrete modal exchange. Unlike the continuous size evolution in the atmosphere, the modal framework represents growth and transfer across modal boundaries in a discretized manner, which can introduce uncertainties in the timing and magnitude of simulated D_g evolution (Mann et al., 2012). These findings emphasize the necessity of benchmarking size-resolved properties predicted by modal schemes against high-resolution observations to constrain their temporal evolution.

https://doi.org/10.5194/egusphere-2026-3636
Preprint. Discussion started: 24 July 2026

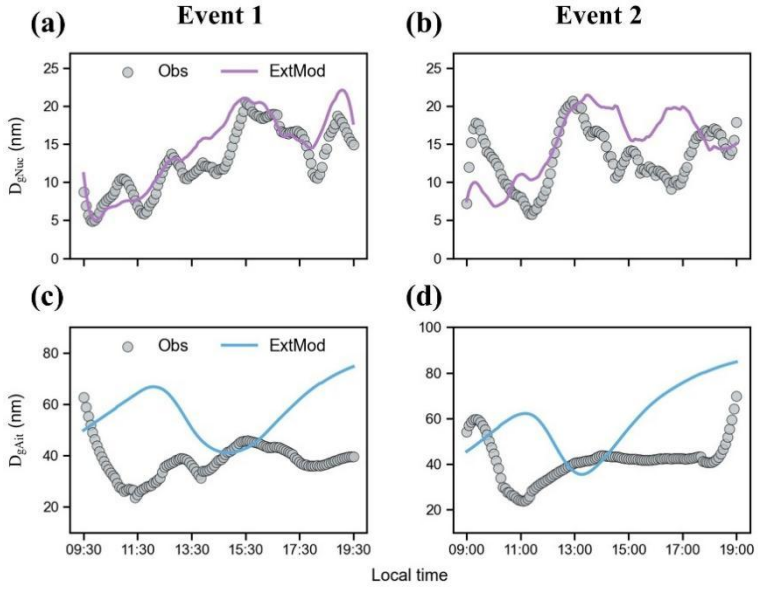

Figure 6. Comparison of the geometric mean diameter (D_g) evolution for Event 1 (left panels) and Event 2 (right panels). (a, b) The D_g of nucleation mode. (c, d) theD_g of Aitken mode. Grey circles represent observationally constrained values derived from the nucleation-resolved decomposition in Sect. 3.1, and solid lines represent ExtMod simulations.

To assess the potential climatic implications of the simulated particle growth, we evaluate the model performance in representing particles large enough to act as potential Cloud Condensation Nuclei (CCN). We analyzed the number concentration of particles larger than 50 nm ($N_{>50}$) as a proxy for CCN-relevant particles, given that particles in this size range are more likely to activate under typical atmospheric supersaturations (Hong et al., 2024; Kerminen et al., 2012; Zhang et al., 2025; Zhu et al., 2021). As shown in Figure 7, both model configurations overestimate $N_{>50}$ in the two events, but the bias is apparently reduced in ExtMod relative to the Base scenario. This improvement is clearly quantified in Table S5. For Event 1, ExtMod reduces the NME from 1.13 to 0.66, the NMB from 1.13 to 0.58, and the RMSE from 7.05×10^3 to 4.90×10^3 relative to the Base scenario. A consistent behavior is found for Event 2, where both scenarios overestimate $N_{>50}$, but ExtMod remains closer to the observations than the Base scenario. The stronger overestimation in the Base scenario is consistent with its overly rapid transfer of particles toward larger diameters, which artificially enhances the number of particles in the CCN-relevant size range. The identical tendency is also observed for $N_{>100}$ (particles larger than 100 nm), indicating that the advantages of ExtMod extend beyond the 50 nm threshold and persists into larger CCN-relevant size ranges. Both scenarios overestimate $N_{>100}$ in the two events, with smaller bias in ExtMod (shown in Fig. S3 and Table S6). These results illustrate that incorporating the early growth dynamics is critical to mitigate the overestimation of particle survival to CCN-relevant sizes (Blichner et al., 2021; Pierce and Adams, 2009). However, the residual positive bias in ExtMod likely reflects the absence of explicit CCN activation and cloud-processing sinks in the present box model, which allows particles that have grown into the CCN-relevant size range to remain in the particle population rather than being activated and removed.

https://doi.org/10.5194/egusphere-2026-3636
Preprint. Discussion started: 24 July 2026

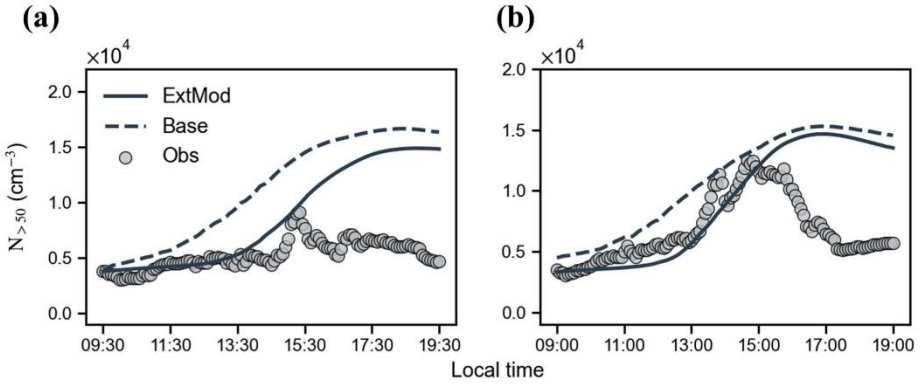

Figure 7. Temporal evolution of particle number concentrations larger than 50 nm ($N_{>50}$) for (a) Event 1 and (b) Event 2. The scatter points represent observational data derived from particle size distributions, while the dashed and solid lines denote the simulation results from the Base scenario and the ExtMod scenario.

3.3 Influence of the Kelvin Effect on Modal Redistribution and Nucleation-Mode Composition

The Kelvin effect plays a pivotal role in governing the dynamics of the initial growth of nanoparticles (Zhang et al., 2012). While this effect is subtle in the Aitken and larger modes, it is expected to be strongest in the nucleation mode, where particle sizes are smallest and condensational growth is therefore most sensitive to particle curvature. To isolate its influence within the extended modal framework, we conducted a sensitivity simulation (denoted as the KelOff scenario) by disabling the Kelvin correction for condensational growth. This comparison allows us to examine how the Kelvin effect alters the temporal evolution of number and mass concentrations in the nucleation, Aitken, and accumulation modes, as well as the chemical composition of the nucleation mode.

Figure 8a–c illustrates that the Kelvin effect substantially modulates the redistribution of particle number among the nucleation, Aitken, and accumulation modes. In the nucleation mode, disabling the Kelvin correction leads to a modest increase in particle number during the active growth period, followed by a more rapid decline after approximately 13:30 local time. This indicates that omitting the thermodynamic barrier imposed by the Kelvin effect allows particles to grow out of the nucleation mode more rapidly rather than remaining confined to the nucleation (Figure 8a). The response is even more pronounced in the Aitken mode, where KelOff produces consistently higher number concentrations than ExtMod, with the deviation curve peaking during the rapid growth stage in the early afternoon (Figure 8b). This shows that the Kelvin effect primarily limits the transfer of particles from the nucleation mode into the Aitken mode by suppressing condensational growth. A smaller but still perceptible enhancement is also found in the accumulation mode, implying that the impact of the Kelvin effect can propagate to larger sizes as growth-induced differences accumulate over time. In general, these results demonstrate that the Kelvin effect does not simply suppress condensational growth of smaller particles, but rather alters the system-wide dynamics by inducing a temporal shift in the accumulation and transfer of particle number within modal schemes.

https://doi.org/10.5194/egusphere-2026-3636
Preprint. Discussion started: 24 July 2026

Moreover, Figure 8d-f reveals that the Kelvin effect exerts a clear influence on the redistribution of aerosol mass among the three modes. In the nucleation mode, KelOff yields a slightly higher mass concentration than ExtMod during the initial growth stage, with the largest positive difference appearing near the peak around 12:00 local time (Figure 8d). Afterwards, the nucleation-mode mass decreases more rapidly in KelOff, indicating that condensable substance is transferred out of this mode more efficiently once particle growth is no longer strongly constrained by curvature effects. This transferred mass is primarily reflected in the Aitken mode, where KelOff produces persistently higher mass concentrations than ExtMod throughout the afternoon (Figure 8e). The enhanced Aitken-mode mass suggests that weakening the Kelvin constraint facilitates the accumulation of condensable vapors onto newly formed particles and accelerates their propagation into adjacent larger mode. A slight increase is also detected in the accumulation mode, implying that the influence of the Kelvin effect can extend to larger particles through the cumulative effect of earlier growth enhancement (Figure 8f). Overall, these results indicate that the Kelvin effect regulates not only how rapidly particles gain mass, but also how that mass is transferred across modes as particle growth proceeds.

A similar response is found for Event 2 (Fig. S4). Disabling the Kelvin correction again enhances the transfer of particle number and mass from the nucleation mode to larger modes, with the most pronounced response appearing in the Aitken mode. The accumulation mode shows a weaker and more delayed sensitivity because it simply reflects the built-up results of how smaller particles grew over time. These parallel findings confirm that the regulatory role of the Kelvin effect on particle growth dynamics is a consistent feature across different NPF events.

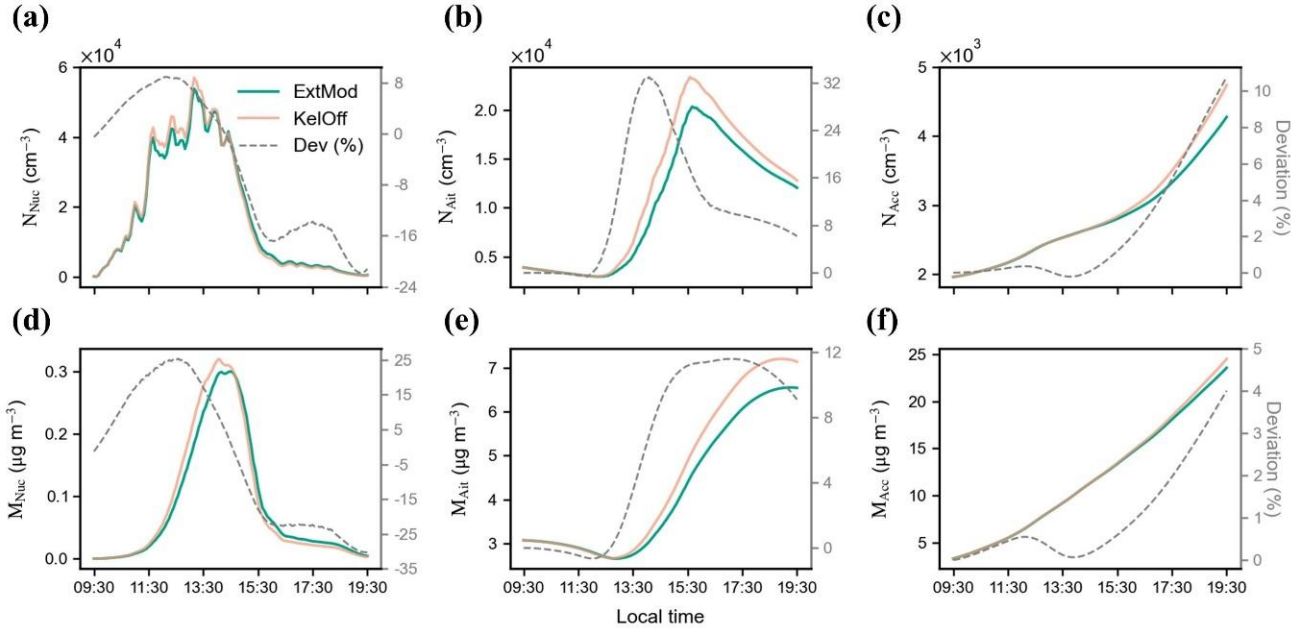

Figure 8. Sensitivity analysis of modal number and mass concentrations to the Kelvin effect for Event 1. Panels (a)–(c) show the temporal evolution of number concentrations in the nucleation, Aitken, and accumulation modes, respectively, and panels (d)–(f) show the corresponding mass concentrations. The green and orange solid lines represent the ExtMod and KelOff simulations, respectively, while the gray dashed lines denote the deviation between KelOff and ExtMod.

https://doi.org/10.5194/egusphere-2026-3636
Preprint. Discussion started: 24 July 2026

The composition of the nucleation-mode mass provides further insight into the mechanism by which the Kelvin effect modifies early particle growth (Figure 9). The organic vapors are categorized according to their effective saturation concentrations at 300 K into ELVOCs ($C^* = 10^{-8}$-10^{-5} μg m^{-3}), LVOCs ($C^* = 10^{-4}$-10^{-1} μg m^{-3}), and SVOCs ($C^* \geq 10^{0}$ μg m^{-3}). Compared with ExtMod, KelOff produces a slightly higher and earlier peak in nucleation-mode mass, increasing the maximum value from approximately 0.302 to 0.317 μg m^{-3}. This mass enhancement is mainly associated with organic vapors, as the nucleation-mode mass is jointly dominated by LVOCs and ELVOCs during the main growth period. During this stage, LVOCs account for about 61% of the nucleation-mode mass in ExtMod, followed by ELVOCs at about 31%, whereas SA and SVOCs contribute only about 6% and 2%, respectively. When the Kelvin correction is disabled, the LVOC contribution increases slightly to about 63%, while the relative contributions of SA and ELVOCs decrease modestly. This shift indicates that the Kelvin effect constrains the condensation of low-volatility organic vapors onto newly formed particles, thereby limiting the organic mass accumulated in the nucleation mode (Colbeck and Lazaridis, 2014; Kiendler-Scharr et al., 2009). Although SA is important during the earliest stage of particle formation, its mass fraction rapidly decreases as organic vapors become the dominant contributors to nucleation-mode growth. Therefore, the Kelvin effect influences modal redistribution not only by changing the rate of condensational growth, but also by regulating the amount of organic material that can be incorporated into the smallest particles.

A broadly similar compositional evolution is also observed for Event 2 (Fig. S5). The nucleation-mode mass is dominated by organic species during the main growth period, with LVOCs and ELVOCs contributing most of the mass, while the relative contribution of SA decreases rapidly after the onset of growth. Compared with ExtMod, KelOff leads to a slightly increased nucleation-mode mass and a modest enhancement in the relative contribution of LVOCs, indicating that the compositional response to the Kelvin effect is qualitatively consistent across both events.

Taken together, the results in Figure 8 and Figure 9 suggest that the influence of the Kelvin effect on modal evolution is mediated primarily through its control over condensational uptake by the smallest particles. By restricting the accumulation of low-volatility organic vapors in the nucleation mode, the Kelvin effect slows the build-up of particle mass and delays the transfer of particles into the Aitken mode. This mechanism explains why the strongest sensitivity appears in the Aitken-mode number and mass concentrations, while the response in the accumulation mode is weaker and more delayed. This interpretation of chemical compositions is also consistent with previous studies using VBS-based representations of organic aerosol evolution, which highlight the dominant role of low-volatility organics in early particle growth (Gao et al., 2017; Li et al., 2023).

https://doi.org/10.5194/egusphere-2026-3636
Preprint. Discussion started: 24 July 2026

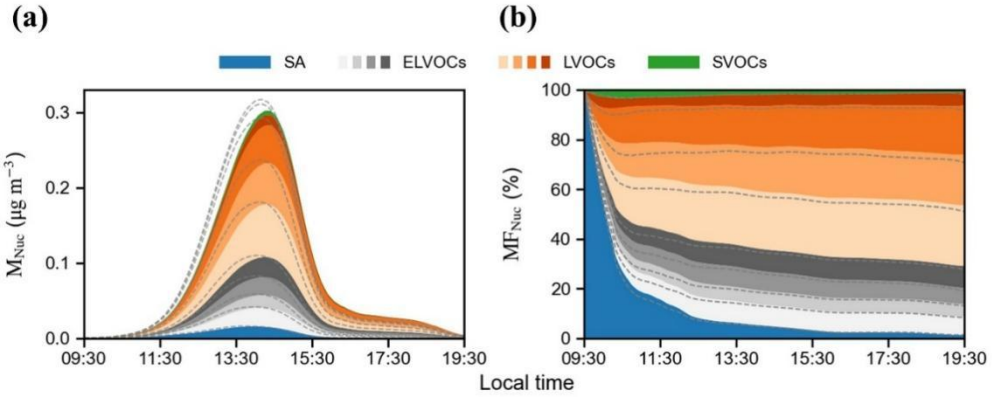

Figure 9. Temporal evolution of the nucleation-mode mass concentration (a) and mass fraction (b) of sulfuric acid (SA) and organic compounds in the ExtMod and KelOff simulations. Colored stacked areas represent the ExtMod results, and gray dashed lines denote the corresponding cumulative contributions in the KelOff simulation. The organic compounds are grouped by saturation concentration (C^* at 300 K) into extremely low-volatility organic compounds (ELVOCs, $C^* = 10^{-8}$-10^{-5} μg m^{-3}), low-volatility organic compounds (LVOCs, $C^* = 10^{-4}$-10^{-1} μg m^{-3}), and semivolatile organic compounds (SVOCs, $C^* \geq 10^{0}$ μg m^{-3}).

3.4 Comparative analysis between modal and sectional schemes

Having validated the model's simulation performance against observation, this section further assesses its fidelity by comparing ExMAD against sectional schemes. Sectional models discretize the particle size distribution into adjacent bins and therefore provide a more explicit representation of PSD shapes, making them a valuable reference for evaluating the structural behavior of modal schemes (Huang et al., 2016; Zhao et al., 2024). To compare the two frameworks under consistent physical conditions, we conducted a comparative simulation between the ExMAD model and the Sec scenario, the latter of which incorporates a state-of-the-art sectional structure (Li et al., 2023). The Sec configuration was implemented with 20, 50, and 100 size bins to examine the sensitivity of the sectional results to bin resolution. Because sectional solutions become less sensitive to discretization as the number of bins increases, the 100-bin configuration (Sec100) was selected as the highest-resolution sectional reference for comparison with ExtMod. To ensure a rigorous comparison, all other model settings (e.g., time step, precursor concentrations and meteorological conditions) were maintained identically.

The comparative results for Event 1 are shown in Figure 10, where panel (a) presents the PSD simulated by Sec100, and panels (b) and (c) compare the temporal evolution of N_{4-25} and N_{25-100}, respectively. 错误!未找到引用源。a shows that Sec100 reproduces the general PSD evolution during the event, while exhibiting a broader size distribution and a faster transfer of particles from the nucleation range to larger diameters. For the sub-25 nm number concentration, ExtMod reproduces the observed evolution more accurately than Sec100, yielding a smaller negative bias and lower overall error (NMB = -0.20 and NME = 0.26 for ExtMod, compared with NMB = -0.63 and NME = 0.64 for Sec100; Table S7). A similar advantage of ExtMod is also seen for Event 2 (Fig. S6b and Table S7), where Sec100 reaches an earlier peak and declines too rapidly afterward, whereas ExtMod better reproduces the observed persistence of N_{4-25}. This result indicates that the modal framework more realistically captures the temporal variability of newly formed particles in the early growth stage. For

https://doi.org/10.5194/egusphere-2026-3636
Preprint. Discussion started: 24 July 2026

N_{25-100}, the two frameworks show comparable model performance but with contrasting biases. ExtMod tends to underestimate the observed concentration, whereas Sec100 exhibits a positive bias and produces a stronger accumulation in this size range. Event 2 shows the same qualitative contrast (Figure S6c), with ExtMod underestimating the magnitude of N_{25-100}, whereas Sec100 produces a stronger and earlier accumulation followed by a rapid decay. Across both events, this contrast suggests that the main difference between the two schemes lies in how they represent particle transfer into, and residence time within, the 25-100 nm size range. Instead, the remaining differences more plausibly reflect structural contrasts between the two frameworks, with ExtMod representing early particle growth and inter-range transfer through continuous modal evolution, whereas Sec100 relies on bin-averaged growth and redistribution across discrete size sections.

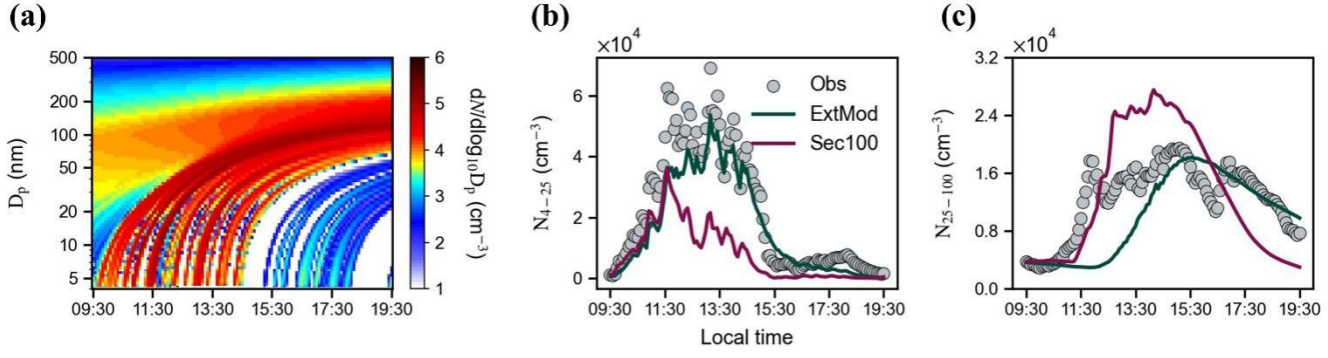

Figure 10. Comparison between the extended modal scheme and the high-resolution sectional scheme for Event 1. Panel (a) shows the particle size distribution (PSD) simulated by the 100-bin sectional configuration (Sec100). Panels (b) and (c) compare the temporal evolution of particle number concentrations in the 4-25 nm (N_{4-25}) and 25-100 nm (N_{25-100}) size ranges, respectively. Grey circles denote observations, and the green and purple lines represent the ExtMod and Sec100 simulations.

Figure 10 further demonstrates that ExtMod captures the short-term variability of N_{4-25} more faithfully than the sectional scheme. In contrast, the Sec100 simulation exhibits a smoother temporal evolution, characterized by an earlier peak and a more rapid decline after the main growth stage. Sectional aerosol models are known to be susceptible to numerical diffusion, especially when particle mass is transferred rapidly across adjacent size bins (Gelbard and Seinfeld, 1980; Whitby and McMurry, 1997; Wu et al., 2021). Additional sensitivity tests using 20-, 50-, and 100-bin sectional configurations show only modest differences in the simulated N_{4-25} and N_{25-100} time series (Fig. S7), indicating that numerical diffusion may contribute to the smoothing of the sectional results, but it is unlikely to be the sole cause of the contrast between the two frameworks. Because the three sectional resolutions produce similar growth trajectories, the remaining discrepancy is more plausibly linked to how the sectional framework represents particle transfer across fixed size intervals during rapid early growth, rather than to bin resolution alone. Together with the reasonable reproduction of nucleation-mode size evolution shown in Figure 6, these results suggest that the advantage of ExtMod arises mainly from its structural treatment of early particle growth and inter-range transfer, rather than from a purely numerical difference in size discretization.

While model performance is critical, computational efficiency is indispensable for practical implementation in three-dimensional atmospheric frameworks. To quantify the computational burden of different schemes, we compared the total runtime of the Base, ExtMod, Sec20, Sec50, and Sec100 configurations. To rule out the contingency of single experiments,

https://doi.org/10.5194/egusphere-2026-3636
Preprint. Discussion started: 24 July 2026

we conducted twenty independent simulations for each scenario, with the averaged computational times summarized in Table 2. The computational cost of the sectional framework increases sharply with bin resolution. Even the coarsest sectional configuration examined here, Sec20, requires 17.68 s, which is 8.5 times the runtime of the Base scenario (2.08 s). The runtime increases further to 36.84 s for Sec50 and 92.66 s for Sec100, corresponding to 17.7 and 44.5 times the cost of the Base configuration, respectively. Such a rapid increase in computational cost would severely constrain the practical application of high-resolution sectional schemes in three-dimensional simulations. By comparison, extending the modal framework from Base to ExtMod increases the average runtime only from 2.08 to 2.13 s, corresponding to an increment of about 2.4%. These results indicate that ExtMod achieves improved representation of NPF dynamics at a subtle additional cost, while remaining far more efficient than the sectional alternatives, thereby confirming its suitability for future large-scale applications.

Table 2. Average computational time of the Base, ExtMod, and sectional configurations (Sec20, Sec50, and Sec100). Values denote the mean runtime from 20 independent simulations performed under identical model settings.

Scenario	Computational time (s)
Base	2.08
ExtMod	2.13
Sec20	17.68
Sec50	36.84
Sec100	92.66

4 Conclusions

In this study, we developed the Extended Modal Aerosol Dynamics Model (ExMADv1.0), which explicitly resolves a nucleation mode to represent the early evolution of particles during NPF events. The gas-particle partitioning in the ExMAD framework accounts for the condensational contribution of organic precursors, which are represented via a Volatility Basis Set (VBS) framework and categorized into volatility bins spanning from extremely low-volatility (ELVOCs) to semi-volatility (SVOCs). The Gauss-Hermite quadrature-based coagulation kernel was extended to account for intra- and inter-modal particle interactions across the nucleation, Aitken, and accumulation modes. Additionally, the framework embeds an analytical size-dependent Kelvin correction and a boundary-aware treatment of particle transfer across adjacent modes, thereby resolving the rapid evolution of nucleation-mode particles from formation through growth into larger size ranges.

This framework is supported by the observed particle size distributions collected in the typical chemical environment of Nanjing, China, which reveal two distinct aerosol populations below 100 nm separated at approximately 25 nm. The observational evidence confirms that an explicit nucleation mode is essential for decoupling the evolution of freshly nucleated particles from background aerosols during NPF events. ExMAD reproduced the observed PSD growth patterns and more faithfully captured the temporal evolution of particle number concentrations, especially in the sub-25 nm size

https://doi.org/10.5194/egusphere-2026-3636
Preprint. Discussion started: 24 July 2026

range. Specifically, our model captured 77% and 85% of the observed N_{4-25} for Event 1 and Event 2, respectively, whereas the default model reproduced only approximately 45%. The model also accurately reproduced the temporal evolution of the geometric mean diameter of the nucleation mode, indicating that the main features of early particle growth were successfully resolved. The event-averaged simulated D_g reached 14.4 and 15.1 nm for Event 1 and Event 2, compared with the observed values of 12.9 and 13.3 nm, respectively. Our sensitivity test further suggests that the Kelvin effect not only acts as a critical thermodynamic constraint on nanoparticle growth but also regulates the transition of these particles to larger modes. Despite the subtle shift in particle partitioning induced by the Kelvin effect, the chemical roles of primary precursors remain robust, with sulfuric acid driving the initial stage and low-volatility organics dominating the subsequent mass accumulation. As a result, the extended scheme improves the representation of particle growth into size ranges relevant for CCN.

Beyond validating the model against observations, this study extended the evaluation to examine the model's performance against sectional schemes. Comparisons with sectional simulations of varying resolutions further highlighted the structural advantages of the extended modal scheme. Relative to the sectional framework, the extended modal scheme better reproduced the short-term variability of sub-25 nm particle number concentrations, whereas the sectional results exhibited an overly smooth temporal evolution. Regarding computational efficiency, ExtMod increases runtime by only about 2.4% relative to the default modal configuration while providing substantially improved representation of NPF dynamics. By contrast, the computational cost of the sectional framework increases sharply with bin resolution, reaching 44.5 times the runtime of the Base configuration for Sec100, which severely limits its practical application in three-dimensional models.

In summary, the extended modal scheme achieves an optimal balance between model performance and computational cost, thus providing a promising candidate for future integration into three-dimensional atmospheric chemical transport models. While the current zero-dimensional box model framework successfully captures the core microphysics of early particle growth, it lacks explicit treatments for CCN activation, regional transport and primary particle emissions. Our future work will focus on incorporating these processes, which are essential for applying the extended modal scheme to comprehensive three-dimensional atmospheric models.

Code and data availability

The source code for the ExMADv1.0 framework and the simulation data are available at https://doi.org/10.5281/zenodo.20773361 (Lin et al., 2026).

Author contributions

JianW and CL conceptualized the study. QL developed the dynamic algorithm and prepared the original draft of the manuscript. JiapW, WN, XQ, YL, XC provided the observational data at the SORPES station and assisted with the data

https://doi.org/10.5194/egusphere-2026-3636
Preprint. Discussion started: 24 July 2026

analysis. JianW, CL, DD and XH provided overarching supervision and critical guidance on the methodology. All authors contributed to the scientific discussion and the editing of the manuscript.

Competing interests

The authors declare that they have no conflict of interest.

Financial support

This research has been supported by the National Natural Science Foundation of China (grant no. 42422505).

References

Ackermann, I. J., Hass, H., Memmesheimer, M., Ebel, A., Binkowski, F. S., and Shankar, U.: Modal aerosol dynamics model for Europe: development and first applications, Atmos. Environ., 32, 2981–2999, https://doi.org/10.1016/S1352-2310(98)00006-5, 1998.

Appel, K. W., Napelenok, S. L., Foley, K. M., Pye, H. O. T., Hogrefe, C., Luecken, D. J., Bash, J. O., Roselle, S. J., Pleim, J. E., Foroutan, H., Hutzell, W. T., Pouliot, G. A., Sarwar, G., Fahey, K. M., Gantt, B., Gilliam, R. C., Heath, N. K., Kang, D., Mathur, R., Schwede, D. B., Spero, T. L., Wong, D. C., and Young, J. O.: Description and evaluation of the Community Multiscale Air Quality (CMAQ) modeling system version 5.1, Geosci. Model Dev., 10, 1703–1732, https://doi.org/10.5194/gmd-10-1703-2017, 2017.

Bauer, S. E., Wright, D. L., Koch, D., Lewis, E. R., McGraw, R., Chang, L.-S., Schwartz, S. E., and Ruedy, R.: MATRIX (Multiconfiguration Aerosol TRacker of mIXing state): an aerosol microphysical module for global atmospheric models, Atmospheric Chem. Phys., 8, 6003–6035, https://doi.org/10.5194/acp-8-6003-2008, 2008.

Bergman, T., Kerminen, V.-M., Korhonen, H., Lehtinen, K. J., Makkonen, R., Arola, A., Mielonen, T., Romakkaniemi, S., Kulmala, M., and Kokkola, H.: Evaluation of the sectional aerosol microphysics module SALSA implementation in ECHAM5-HAM aerosol-climate model, Geosci. Model Dev., 5, 845–868, https://doi.org/10.5194/gmd-5-845-2012, 2012.

Binkowski, F. S. and Roselle, S. J.: Models-3 Community Multiscale Air Quality (CMAQ) model aerosol component 1. Model description, J. Geophys. Res. Atmospheres, 108, https://doi.org/10.1029/2001JD001409, 2003.

Binkowski, F. S. and Shankar, U.: The Regional Particulate Matter Model: 1. Model description and preliminary results, J. Geophys. Res. Atmospheres, 100, 26191–26209, https://doi.org/10.1029/95JD02093, 1995.

Blichner, S. M., Sporre, M. K., Makkonen, R., and Berntsen, T. K.: Implementing a sectional scheme for early aerosol growth from new particle formation in the Norwegian Earth System Model v2: comparison to observations and climate impacts, Geosci. Model Dev., 14, 3335–3359, https://doi.org/10.5194/gmd-14-3335-2021, 2021.

https://doi.org/10.5194/egusphere-2026-3636
Preprint. Discussion started: 24 July 2026

Bousiotis, D., Brean, J., Pope, F. D., Dall'Osto, M., Querol, X., Alastuey, A., Perez, N., Petäjä, T., Massling, A., Nøjgaard, J. K., Nordstrøm, C., Kouvarakis, G., Vratolis, S., Eleftheriadis, K., Niemi, J. V., Portin, H., Wiedensohler, A., Weinhold, K., Merkel, M., Tuch, T., and Harrison, R. M.: The effect of meteorological conditions and atmospheric composition in the occurrence and development of new particle formation (NPF) events in Europe, Atmospheric Chem. Phys., 21, 3345–3370, https://doi.org/10.5194/acp-21-3345-2021, 2021.

Boy, M., Hellmuth, O., Korhonen, H., Nilsson, E. D., ReVelle, D., Turnipseed, A., Arnold, F., and Kulmala, M.: MALTE – model to predict new aerosol formation in the lower troposphere, Atmospheric Chem. Phys., 6, 4499–4517, https://doi.org/10.5194/acp-6-4499-2006, 2006.

Cai, C., Zhang, X., Wang, K., Zhang, Y., Wang, L., Zhang, Q., Duan, F., He, K., and Yu, S.-C.: Incorporation of new particle formation and early growth treatments into WRF/Chem: Model improvement, evaluation, and impacts of anthropogenic aerosols over East Asia, Atmos. Environ., 124, 262–284, https://doi.org/10.1016/j.atmosenv.2015.05.046, 2016.

Cai, J., Chu, B., Yao, L., Yan, C., Heikkinen, L. M., Zheng, F., Li, C., Fan, X., Zhang, S., Yang, D., Wang, Y., Kokkonen, T. V., Chan, T., Zhou, Y., Dada, L., Liu, Y., He, H., Paasonen, P., Kujansuu, J. T., Petäjä, T., Mohr, C., Kangasluoma, J., Bianchi, F., Sun, Y., Croteau, P. L., Worsnop, D. R., Kerminen, V.-M., Du, W., Kulmala, M., and Daellenbach, K. R.: Size-segregated particle number and mass concentrations from different emission sources in urban Beijing, Atmospheric Chem. Phys., 20, 12721–12740, https://doi.org/10.5194/acp-20-12721-2020, 2020.

Cai, R. and Jiang, J.: A new balance formula to estimate new particle formation rate: reevaluating the effect of coagulation scavenging, Atmospheric Chem. Phys., 17, 12659–12675, https://doi.org/10.5194/acp-17-12659-2017, 2017.

Cai, R., Chandra, I., Yang, D., Yao, L., Fu, Y., Li, X., Lu, Y., Luo, L., Hao, J., Ma, Y., Wang, L., Zheng, J., Seto, T., and Jiang, J.: Estimating the influence of transport on aerosol size distributions during new particle formation events, Atmospheric Chem. Phys., 18, 16587–16599, https://doi.org/10.5194/acp-18-16587-2018, 2018.

Cai, R., Yan, C., Yang, D., Yin, R., Lu, Y., Deng, C., Fu, Y., Ruan, J., Li, X., Kontkanen, J., Zhang, Q., Kangasluoma, J., Ma, Y., Hao, J., Worsnop, D. R., Bianchi, F., Paasonen, P., Kerminen, V.-M., Liu, Y., Wang, L., Zheng, J., Kulmala, M., and Jiang, J.: Sulfuric acid–amine nucleation in urban Beijing, Atmospheric Chem. Phys., 21, 2457–2468, https://doi.org/10.5194/acp-21-2457-2021, 2021.

Chen, L., Qi, X., Niu, G., Li, Y., Liu, C., Lai, S., Liu, Y., Nie, W., Yan, C., Wang, J., Chi, X., Paasonen, P., Hussein, T., Lehtipalo, K., Kerminen, V.-M., Petäjä, T., Kulmala, M., and Ding, A.: High Concentration of Atmospheric Sub-3 nm Particles in Polluted Environment of Eastern China: New Particle Formation and Traffic Emission, J. Geophys. Res. Atmospheres, 128, e2023JD039669, https://doi.org/10.1029/2023JD039669, 2023.

Chen, X., Wang, Z., Li, J., Yang, W., Chen, H., Wang, Z., Hao, J., Ge, B., Wang, D., and Huang, H.: Simulation on different response characteristics of aerosol particle number concentration and mass concentration to emission changes over mainland China, Sci. Total Environ., 643, 692–703, https://doi.org/10.1016/j.scitotenv.2018.06.181, 2018.

https://doi.org/10.5194/egusphere-2026-3636
Preprint. Discussion started: 24 July 2026

Chen, X., Yu, F., Yang, W., Sun, Y., Chen, H., Du, W., Zhao, J., Wei, Y., Wei, L., Du, H., Wang, Z., Wu, Q., Li, J., An, J., and Wang, Z.: Global–regional nested simulation of particle number concentration by combing microphysical processes with an evolving organic aerosol module, Atmospheric Chem. Phys., 21, 9343–9366, https://doi.org/10.5194/acp-21-9343-2021, 2021.

Chen, Y., Haywood, J., Wang, Y., Malavelle, F., Jordan, G., Partridge, D., Fieldsend, J., De Leeuw, J., Schmidt, A., Cho, N., Oreopoulos, L., Platnick, S., Grosvenor, D., Field, P., and Lohmann, U.: Machine learning reveals climate forcing from aerosols is dominated by increased cloud cover, Nat. Geosci., 15, 609–614, https://doi.org/10.1038/s41561-022-00991-6, 2022.

Colbeck, I. and Lazaridis, M.: Aerosol Science: Technology and Applications, John Wiley & Sons, 522 pp., 2014.

Dai, L., Wang, H., Zhou, L., An, J., Tang, L., Lu, C., Yan, W., Liu, R., Kong, S., Chen, M., Lee, S., and Yu, H.: Regional and local new particle formation events observed in the Yangtze River Delta region, China, https://doi.org/10.1002/2016JD026030, 2017.

Dal Maso, M., Kulmala, M., Riipinen, I., and Wagner, R.: Formation and growth of fresh atmospheric aerosols: Eight years of aerosol size distribution data from SMEAR II, Hyytiälä, Finland, Boreal Environ. Res., 10, 323–336, 2005.

Deng, C., Fu, Y., Dada, L., Yan, C., Cai, R., Yang, D., Zhou, Y., Yin, R., Lu, Y., Li, X., Qiao, X., Fan, X., Nie, W., Kontkanen, J., Kangasluoma, J., Chu, B., Ding, A., Kerminen, V.-M., Paasonen, P., Worsnop, D. R., Bianchi, F., Liu, Y., Zheng, J., Wang, L., Kulmala, M., and Jiang, J.: Seasonal Characteristics of New Particle Formation and Growth in Urban Beijing, Environ. Sci. Technol., 54, 8547–8557, https://doi.org/10.1021/acs.est.0c00808, 2020.

Deng, C., Li, Y., Yan, C., Wu, J., Cai, R., Wang, D., Liu, Y., Kangasluoma, J., Kerminen, V.-M., Kulmala, M., and Jiang, J.: Measurement report: Size distributions of urban aerosols down to 1 nm from long-term measurements, Atmospheric Chem. Phys., 22, 13569–13580, https://doi.org/10.5194/acp-22-13569-2022, 2022.

Ding, A., Nie, W., Huang, X., Chi, X., Sun, J., Kerminen, V.-M., Xu, Z., Guo, W., Petäjä, T., Yang, X., Kulmala, M., and Fu, C.: Long-term observation of air pollution-weather/climate interactions at the SORPES station: a review and outlook, Front. Environ. Sci. Eng., 10, 15, https://doi.org/10.1007/s11783-016-0877-3, 2016.

Ding, A. J., Fu, C. B., Yang, X. Q., Sun, J. N., Zheng, L. F., Xie, Y. N., Herrmann, E., Nie, W., Petäjä, T., Kerminen, V.-M., and Kulmala, M.: Ozone and fine particle in the western Yangtze River Delta: an overview of 1 yr data at the SORPES station, Atmospheric Chem. Phys., 13, 5813–5830, https://doi.org/10.5194/acp-13-5813-2013, 2013.

Donahue, N. M., Epstein, S. A., Pandis, S. N., and Robinson, A. L.: A two-dimensional volatility basis set: 1. organic-aerosol mixing thermodynamics, Atmospheric Chem. Phys., 11, 3303–3318, https://doi.org/10.5194/acp-11-3303-2011, 2011.

Fierce, L., Robey, A. J., and Hamilton, C.: Simulating near-field enhancement in transmission of airborne viruses with a quadrature-based model, Indoor Air, 31, 1843–1859, https://doi.org/10.1111/ina.12900, 2021.

https://doi.org/10.5194/egusphere-2026-3636
Preprint. Discussion started: 24 July 2026

Fierce, L., Yao, Y., Easter, R., Ma, P.-L., Sun, J., Wan, H., and Zhang, K.: Quantifying structural errors in cloud condensation nuclei activity from reduced representation of aerosol size distributions, J. Aerosol Sci., 181, 106388, https://doi.org/10.1016/j.jaerosci.2024.106388, 2024.

Forster, P. M., Forster, H. I., Evans, M. J., Gidden, M. J., Jones, C. D., Keller, C. A., Lamboll, R. D., Quéré, C. L., Rogelj, J., Rosen, D., Schleussner, C.-F., Richardson, T. B., Smith, C. J., and Turnock, S. T.: Current and future global climate impacts resulting from COVID-19, Nat. Clim. Change, 10, 913–919, https://doi.org/10.1038/s41558-020-0883-0, 2020.

Fuzzi, S., Baltensperger, U., Carslaw, K., Decesari, S., Denier van der Gon, H., Facchini, M. C., Fowler, D., Koren, I., Langford, B., Lohmann, U., Nemitz, E., Pandis, S., Riipinen, I., Rudich, Y., Schaap, M., Slowik, J. G., Spracklen, D. V., Vignati, E., Wild, M., Williams, M., and Gilardoni, S.: Particulate matter, air quality and climate: lessons learned and future needs, Atmospheric Chem. Phys., 15, 8217–8299, https://doi.org/10.5194/acp-15-8217-2015, 2015.

Gao, C. Y., Tsigaridis, K., and Bauer, S. E.: MATRIX-VBS (v1.0): implementing an evolving organic aerosol volatility in an aerosol microphysics model, Geosci. Model Dev., 10, 751–764, https://doi.org/10.5194/gmd-10-751-2017, 2017.

Gelbard, F. and Seinfeld, J. H.: Simulation of multicomponent aerosol dynamics, J. Colloid Interface Sci., 78, 485–501, https://doi.org/10.1016/0021-9797(80)90587-1, 1980.

Gierens, R. T., Laakso, L., Mogensen, D., Vakkari, V., Beukes, J. P., van Zyl, P. G., Hakola, H., Guenther, A., Pienaar, J. J., and Boy, M.: Modelling new particle formation events in the South African savannah, South Afr. J. Sci., 110, 01–12, 2014.

Hong, J., Ma, J., Ma, N., Shi, J., Xu, W., Zhang, G., Zhu, S., Zhang, S., Tang, M., Pan, X., Xie, L., Li, G., Kuhn, U., Yan, C., Qi, X., Zha, Q., Nie, W., Tao, J., He, Y., Zhou, Y., Sun, Y., Xu, H., Liu, L., Cai, R., Zhou, G., Kuang, Y., Yuan, B., Wang, Q., Petäjä, T., Kerminen, V.-M., Kulmala, M., Cheng, Y., and Su, H.: Low Hygroscopicity of Newly Formed Particles on the North China Plain and Its Implications for Nanoparticle Growth, Geophys. Res. Lett., 51, e2023GL107516, https://doi.org/10.1029/2023GL107516, 2024.

Huang, X., Zhou, L., Ding, A., Qi, X., Nie, W., Wang, M., Chi, X., Petäjä, T., Kerminen, V.-M., Roldin, P., Rusanen, A., Kulmala, M., and Boy, M.: Comprehensive modelling study on observed new particle formation at the SORPES station in Nanjing, China, Atmospheric Chem. Phys., 16, 2477–2492, https://doi.org/10.5194/acp-16-2477-2016, 2016.

Huang, X., Ding, K., Liu, J., Wang, Z., Tang, R., Xue, L., Wang, H., Zhang, Q., Tan, Z.-M., Fu, C., Davis, S. J., Andreae, M. O., and Ding, A.: Smoke-weather interaction affects extreme wildfires in diverse coastal regions, Science, 379, 457–461, https://doi.org/10.1126/science.add9843, 2023.

Jacquot, O. and Sartelet, K.: Numerical investigations on the modelling of ultrafine particles in SSH-aerosol-v1.3a: size resolution and redistribution, Geosci. Model Dev., 18, 3965–3984, https://doi.org/10.5194/gmd-18-3965-2025, 2025.

Jia, H. and Quaas, J.: Nonlinearity of the cloud response postpones climate penalty of mitigating air pollution in polluted regions, Nat. Clim. Change, 13, 943–950, https://doi.org/10.1038/s41558-023-01775-5, 2023.

Jokinen, T., Sipilä, M., Richters, S., Kerminen, V.-M., Paasonen, P., Stratmann, F., Worsnop, D., Kulmala, M., Ehn, M., Herrmann, H., and Berndt, T.: Rapid Autoxidation Forms Highly Oxidized RO2 Radicals in the Atmosphere, Angew. Chem. Int. Ed., 53, 14596–14600, https://doi.org/10.1002/anie.201408566, 2014.

https://doi.org/10.5194/egusphere-2026-3636
Preprint. Discussion started: 24 July 2026

Kaiser, J. C., Hendricks, J., Righi, M., Riemer, N., Zaveri, R. A., Metzger, S., and Aquila, V.: The MESSy aerosol submodel MADE3 (v2.0b): description and a box model test, Geosci. Model Dev., 7, 1137–1157, https://doi.org/10.5194/gmd-7-1137-2014, 2014.

Kerminen, V.-M., Paramonov, M., Anttila, T., Riipinen, I., Fountoukis, C., Korhonen, H., Asmi, E., Laakso, L., Lihavainen, H., Swietlicki, E., Svenningsson, B., Asmi, A., Pandis, S. N., Kulmala, M., and Petäjä, T.: Cloud condensation nuclei production associated with atmospheric nucleation: a synthesis based on existing literature and new results, Atmospheric Chem. Phys., 12, 12037–12059, https://doi.org/10.5194/acp-12-12037-2012, 2012.

Kerminen, V.-M., Chen, X., Vakkari, V., Petäjä, T., Kulmala, M., and Bianchi, F.: Atmospheric new particle formation and growth: review of field observations, Environ. Res. Lett., 13, 103003, https://doi.org/10.1088/1748-9326/aadf3c, 2018.

Kiendler-Scharr, A., Wildt, J., Maso, M. D., Hohaus, T., Kleist, E., Mentel, T. F., Tillmann, R., Uerlings, R., Schurr, U., and Wahner, A.: New particle formation in forests inhibited by isoprene emissions, Nature, 461, 381–384, https://doi.org/10.1038/nature08292, 2009.

Korhonen, H., Sihto, S.-L., Kerminen, V.-M., and Lehtinen, K. E. J.: Evaluation of the accuracy of analysis tools for atmospheric new particle formation, Atmospheric Chem. Phys., 11, 3051–3066, https://doi.org/10.5194/acp-11-3051-2011, 2011.

Kulmala, M., Vehkamäki, H., Petäjä, T., Dal Maso, M., Lauri, A., Kerminen, V.-M., Birmili, W., and McMurry, P. H.: Formation and growth rates of ultrafine atmospheric particles: a review of observations, J. Aerosol Sci., 35, 143–176, https://doi.org/10.1016/j.jaerosci.2003.10.003, 2004.

Kulmala, M., Petäjä, T., Nieminen, T., Sipilä, M., Manninen, H. E., Lehtipalo, K., Dal Maso, M., Aalto, P. P., Junninen, H., Paasonen, P., Riipinen, I., Lehtinen, K. E. J., Laaksonen, A., and Kerminen, V.-M.: Measurement of the nucleation of atmospheric aerosol particles, Nat. Protoc., 7, 1651–1667, https://doi.org/10.1038/nprot.2012.091, 2012.

Kulmala, M., Kerminen, V.-M., Petäjä, T., J. Ding, A., and Wang, L.: Atmospheric gas-to-particle conversion: why NPF events are observed in megacities?, Faraday Discuss., 200, 271–288, https://doi.org/10.1039/C6FD00257A, 2017.

Kulmala, M., Cai, R., Stolzenburg, D., Zhou, Y., Dada, L., Guo, Y., Yan, C., Petäjä, T., Jiang, J., and Kerminen, V.-M.: The contribution of new particle formation and subsequent growth to haze formation, Environ. Sci. Atmospheres, 2, 352–361, https://doi.org/10.1039/D1EA00096A, 2022.

Kürten, A., Li, C., Bianchi, F., Curtius, J., Dias, A., Donahue, N. M., Duplissy, J., Flagan, R. C., Hakala, J., Jokinen, T., Kirkby, J., Kulmala, M., Laaksonen, A., Lehtipalo, K., Makhmutov, V., Onnela, A., Rissanen, M. P., Simon, M., Sipilä, M., Stozhkov, Y., Tröstl, J., Ye, P., and McMurry, P. H.: New particle formation in the sulfuric acid–dimethylamine–water system: reevaluation of CLOUD chamber measurements and comparison to an aerosol nucleation and growth model, Atmospheric Chem. Phys., 18, 845–863, https://doi.org/10.5194/acp-18-845-2018, 2018.

Lauer, A., Hendricks, J., Ackermann, I., Schell, B., Hass, H., and Metzger, S.: Simulating aerosol microphysics with the ECHAM/MADE GCM – Part I: Model description and comparison with observations, Atmospheric Chem. Phys., 5, 3251–3276, https://doi.org/10.5194/acp-5-3251-2005, 2005.

https://doi.org/10.5194/egusphere-2026-3636
Preprint. Discussion started: 24 July 2026

Lee, K. W., Chen, J., and Gieseke, J. A.: Log-Normally Preserving Size Distribution for Brownian Coagulation in the Free-Molecule Regime, Aerosol Sci. Technol., 3, 53–62, https://doi.org/10.1080/02786828408958993, 1984.

Lee, Y. H., Pierce, J. R., and Adams, P. J.: Representation of nucleation mode microphysics in a global aerosol model with sectional microphysics, Geosci. Model Dev., 6, 1221–1232, https://doi.org/10.5194/gmd-6-1221-2013, 2013.

Li, C. and Cai, R.: Tutorial: The discrete-sectional method to simulate an evolving aerosol, J. Aerosol Sci., 150, 105615, https://doi.org/10.1016/j.jaerosci.2020.105615, 2020.

Li, C., Li, Y., Li, X., Cai, R., Fan, Y., Qiao, X., Yin, R., Yan, C., Guo, Y., Liu, Y., Zheng, J., Kerminen, V.-M., Kulmala, M., Xiao, H., and Jiang, J.: Comprehensive simulations of new particle formation events in Beijing with a cluster dynamics–multicomponent sectional model, Atmospheric Chem. Phys., 23, 6879–6896, https://doi.org/10.5194/acp-23-6879-2023, 2023.

Lin, Q., Wang, J., Li, C., Huang, X., Wang, J., Nie, W., Liu, Y., Wang, J., Tian, Z., Liu, C., and Ding, A.: Simulation of the Steady Mixing State of Black Carbon With a Two-Dimensional Sectional Model, J. Geophys. Res. Atmospheres, 129, e2024JD041851, https://doi.org/10.1029/2024JD041851, 2024.

Lin, Q., Wang, J., Li, C., Ding, D., Wang, J., Nie, W., Qi, X., Liu, Y., Chi, X., and Huang, X.: Source code for the Extended Modal Aerosol Dynamics Model (ExMAD), Zenodo [code], https://doi.org/10.5281/zenodo.20773361, 2026.

Liu, X., Easter, R. C., Ghan, S. J., Zaveri, R., Rasch, P., Shi, X., Lamarque, J.-F., Gettelman, A., Morrison, H., Vitt, F., Conley, A., Park, S., Neale, R., Hannay, C., Ekman, A. M. L., Hess, P., Mahowald, N., Collins, W., Iacono, M. J., Bretherton, C. S., Flanner, M. G., and Mitchell, D.: Toward a minimal representation of aerosols in climate models: description and evaluation in the Community Atmosphere Model CAM5, Geosci. Model Dev., 5, 709–739, https://doi.org/10.5194/gmd-5-709-2012, 2012.

Liu, X., Ma, P.-L., Wang, H., Tilmes, S., Singh, B., Easter, R. C., Ghan, S. J., and Rasch, P. J.: Description and evaluation of a new four-mode version of the Modal Aerosol Module (MAM4) within version 5.3 of the Community Atmosphere Model, Geosci. Model Dev., 9, 505–522, https://doi.org/10.5194/gmd-9-505-2016, 2016.

Liu, Y., Nie, W., Li, Y., Ge, D., Liu, C., Xu, Z., Chen, L., Wang, T., Wang, L., Sun, P., Qi, X., Wang, J., Xu, Z., Yuan, J., Yan, C., Zhang, Y., Huang, D., Wang, Z., Donahue, N. M., Worsnop, D., Chi, X., Ehn, M., and Ding, A.: Formation of condensable organic vapors from anthropogenic and biogenic volatile organic compounds (VOCs) is strongly perturbed by NO_x in eastern China, Atmospheric Chem. Phys., 21, 14789–14814, https://doi.org/10.5194/acp-21-14789-2021, 2021.

Liu, Y., Liu, C., Nie, W., Li, Y., Ge, D., Chen, L., Zhu, C., Wang, L., Zhang, Y., Liu, T., Qi, X., Wang, J., Huang, D., Wang, Z., Yan, C., Chi, X., and Ding, A.: Exploring condensable organic vapors and their co-occurrence with $PM_{2.5}$ and O_3 in winter in Eastern China, Environ. Sci. Atmospheres, 3, 282–297, https://doi.org/10.1039/D2EA00143H, 2023.

Liu, Y., Nie, W., Qi, X., Li, Y., Xu, T., Liu, C., Ge, D., Chen, L., Niu, G., Wang, J., Yang, L., Wang, L., Zhu, C., Wang, J., Zhang, Y., Liu, T., Zha, Q., Yan, C., Ye, C., Zhang, G., Hu, R., Huang, R.-J., Chi, X., Zhu, T., and Ding, A.: The Pivotal Role of Heavy Terpenes and Anthropogenic Interactions in New Particle Formation on the Southeastern Qinghai-Tibet Plateau, Environ. Sci. Technol., 58, 19748–19761, https://doi.org/10.1021/acs.est.4c04112, 2024.

https://doi.org/10.5194/egusphere-2026-3636
Preprint. Discussion started: 24 July 2026

Mäkelä, J. M., Aalto, P., Jokinen, V., Pohja, T., Nissinen, A., Palmroth, S., Markkanen, T., Seitsonen, K., Lihavainen, H., and Kulmala, M.: Observations of ultrafine aerosol particle formation and growth in boreal forest, Geophys. Res. Lett., 24, 1219–1222, https://doi.org/10.1029/97GL00920, 1997.

Mann, G. W., Carslaw, K. S., Ridley, D. A., Spracklen, D. V., Pringle, K. J., Merikanto, J., Korhonen, H., Schwarz, J. P., Lee, L. A., Manktelow, P. T., Woodhouse, M. T., Schmidt, A., Breider, T. J., Emmerson, K. M., Reddington, C. L., Chipperfield, M. P., and Pickering, S. J.: Intercomparison of modal and sectional aerosol microphysics representations within the same 3-D global chemical transport model, Atmospheric Chem. Phys., 12, 4449–4476, https://doi.org/10.5194/acp-12-4449-2012, 2012.

Mao, J., Yu, F., Murphy, B. N., An, J., Zhang, Y., Luo, G., Lin, S., and Hallar, A. G.: Improved Simulation of Particle Number Concentrations Over the US: Integrating a Size-Resolved Advanced Particle Microphysics Model Into CMAQ, J. Geophys. Res. Atmospheres, 130, e2025JD044021, https://doi.org/10.1029/2025JD044021, 2025.

Matsui, H., Koike, M., Kondo, Y., Takegawa, N., Wiedensohler, A., Fast, J. D., and Zaveri, R. A.: Impact of new particle formation on the concentrations of aerosols and cloud condensation nuclei around Beijing, J. Geophys. Res. Atmospheres, 116, https://doi.org/10.1029/2011JD016025, 2011.

McErlich, C., Goddard, F., Aves, A., Hardacre, C., Evangeliou, N., Hewitt, A. J., and Revell, L. E.: Description and evaluation of airborne microplastics in the United Kingdom Earth System Model (UKESM1.1) using GLOMAP-mode, Geosci. Model Dev., 18, 8827–8854, https://doi.org/10.5194/gmd-18-8827-2025, 2025.

McGraw, R.: Description of Aerosol Dynamics by the Quadrature Method of Moments, Aerosol Sci. Technol., 27, 255–265, https://doi.org/10.1080/02786829708965471, 1997.

McGraw, R. and Wright, D. L.: Chemically resolved aerosol dynamics for internal mixtures by the quadrature method of moments, J. Aerosol Sci., 34, 189–209, https://doi.org/10.1016/S0021-8502(02)00157-X, 2003.

Merikanto, J., Spracklen, D. V., Mann, G. W., Pickering, S. J., and Carslaw, K. S.: Impact of nucleation on global CCN, Atmospheric Chem. Phys., 9, 8601–8616, https://doi.org/10.5194/acp-9-8601-2009, 2009.

Nie, W., Yan, C., Huang, D. D., Wang, Z., Liu, Y., Qiao, X., Guo, Y., Tian, L., Zheng, P., Xu, Z., Li, Y., Xu, Z., Qi, X., Sun, P., Wang, J., Zheng, F., Li, X., Yin, R., Dallenbach, K. R., Bianchi, F., Petäjä, T., Zhang, Y., Wang, M., Schervish, M., Wang, S., Qiao, L., Wang, Q., Zhou, M., Wang, H., Yu, C., Yao, D., Guo, H., Ye, P., Lee, S., Li, Y. J., Liu, Y., Chi, X., Kerminen, V.-M., Ehn, M., Donahue, N. M., Wang, T., Huang, C., Kulmala, M., Worsnop, D., Jiang, J., and Ding, A.: Secondary organic aerosol formed by condensing anthropogenic vapours over China's megacities, Nat. Geosci., 15, 255–261, https://doi.org/10.1038/s41561-022-00922-5, 2022.

Olenius, T. and Riipinen, I.: Molecular-resolution simulations of new particle formation: Evaluation of common assumptions made in describing nucleation in aerosol dynamics models, Aerosol Sci. Technol., 51, 397–408, https://doi.org/10.1080/02786826.2016.1262530, 2017.

Patoulias, D. and Pandis, S. N.: Simulation of the effects of low-volatility organic compounds on aerosol number concentrations in Europe, Atmospheric Chem. Phys., 22, 1689–1706, https://doi.org/10.5194/acp-22-1689-2022, 2022.

https://doi.org/10.5194/egusphere-2026-3636
Preprint. Discussion started: 24 July 2026

Pierce, J. R. and Adams, P. J.: Uncertainty in global CCN concentrations from uncertain aerosol nucleation and primary emission rates, Atmospheric Chem. Phys., 9, 1339–1356, https://doi.org/10.5194/acp-9-1339-2009, 2009.

Qi, X., Zhu, C., Chen, L., Chi, X., Wang, J., Niu, G., Lai, S., Nie, W., Zhu, Y., Huang, X., Kokkonen, T. V., Petäjä, T., Kerminen, V.-M., Kulmala, M., and Ding, A.: Aerosol-Cloud Interactions Near Cloud Base Deteriorating the Haze Pollution in East China, Geophys. Res. Lett., 51, e2024GL109975, https://doi.org/10.1029/2024GL109975, 2024.

Qi, X. M., Ding, A. J., Nie, W., Petäjä, T., Kerminen, V.-M., Herrmann, E., Xie, Y. N., Zheng, L. F., Manninen, H., Aalto, P., Sun, J. N., Xu, Z. N., Chi, X. G., Huang, X., Boy, M., Virkkula, A., Yang, X.-Q., Fu, C. B., and Kulmala, M.: Aerosol size distribution and new particle formation in the western Yangtze River Delta of China: 2 years of measurements at the SORPES station, Atmospheric Chem. Phys., 15, 12445–12464, https://doi.org/10.5194/acp-15-12445-2015, 2015.

Riemer, N., Ault, A. P., West, M., Craig, R. L., and Curtis, J. H.: Aerosol Mixing State: Measurements, Modeling, and Impacts, Rev. Geophys., 57, 187–249, https://doi.org/10.1029/2018RG000615, 2019.

Seinfeld, J. H. and Pandis, S. N.: Atmospheric Chemistry and Physics: From Air Pollution to Climate Change, John Wiley & Sons, 1146 pp., 2016.

Semeniuk, K. and Dastoor, A.: Current State of Atmospheric Aerosol Thermodynamics and Mass Transfer Modeling: A Review, Atmosphere, 11, 156, https://doi.org/10.3390/atmos11020156, 2020.

Shen, J., Yu, M., Chan, T. L., Tu, C., and Liu, Y.: Efficient Method of Moments for Simulating Atmospheric Aerosol Growth: Model Description, Verification, and Application, J. Geophys. Res. Atmospheres, 125, e2019JD032172, https://doi.org/10.1029/2019JD032172, 2020.

Shrivastava, M., Fast, J., Easter, R., Gustafson, W. I. J., Zaveri, R. A., Jimenez, J. L., Saide, P., and Hodzic, A.: Modeling organic aerosols in a megacity: comparison of simple and complex representations of the volatility basis set approach, Atmospheric Chem. Phys., 11, 6639–6662, https://doi.org/10.5194/acp-11-6639-2011, 2011.

Song, Y., Wei, J., Zhao, W., Ding, J., Pei, X., Zhang, F., Xu, Z., Shi, R., Wei, Y., Zhang, L., Jin, L., and Wang, Z.: Measurement report: Size-resolved particle effective density measured by an AAC-SMPS and implications for chemical composition, Atmospheric Chem. Phys., 25, 4755–4766, https://doi.org/10.5194/acp-25-4755-2025, 2025.

Spracklen, D. V., Carslaw, K. S., Pöschl, U., Rap, A., and Forster, P. M.: Global cloud condensation nuclei influenced by carbonaceous combustion aerosol, Atmospheric Chem. Phys., 11, 9067–9087, https://doi.org/10.5194/acp-11-9067-2011, 2011.

Steffen, W., Sanderson, A., Tyson, P., Jäger, J., Matson, P., Moore, B., Oldfield, F., Richardson, K., Schellnhuber, H. J., Turner, B. L., and Wasson, R. J. (Eds.): Planetary Machinery: The Dynamics of the Earth System Prior to Significant Human Influence, in: Global Change and the Earth System: A Planet Under Pressure, Springer, Berlin, Heidelberg, 11–80, https://doi.org/10.1007/3-540-26607-0_2, 2005.

Stier, P., Feichter, J., Kinne, S., Kloster, S., Vignati, E., Wilson, J., Ganzeveld, L., Tegen, I., Werner, M., Balkanski, Y., Schulz, M., Boucher, O., Minikin, A., and Petzold, A.: The aerosol-climate model ECHAM5-HAM, Atmospheric Chem. Phys., 5, 1125–1156, https://doi.org/10.5194/acp-5-1125-2005, 2005.

https://doi.org/10.5194/egusphere-2026-3636
Preprint. Discussion started: 24 July 2026

Stolzenburg, M. R., McMurry, P. H., Sakurai, H., Smith, J. N., Mauldin III, R. L., Eisele, F. L., and Clement, C. F.: Growth rates of freshly nucleated atmospheric particles in Atlanta, J. Geophys. Res. Atmospheres, 110, https://doi.org/10.1029/2005JD005935, 2005.

Tang, L., Feng, Z., Shang, D., Zeng, L., Wu, Z., Wang, H., Chen, S., Li, X., Zeng, L., Hu, J., and Hu, M.: Ongoing uncoordinated anthropogenic emission abatement promotes atmospheric new particle growth in a Chinese megacity, Nat. Commun., 16, 6720, https://doi.org/10.1038/s41467-025-62011-6, 2025.

Tegen, I., Neubauer, D., Ferrachat, S., Siegenthaler-Le Drian, C., Bey, I., Schutgens, N., Stier, P., Watson-Parris, D., Stanelle, T., Schmidt, H., Rast, S., Kokkola, H., Schultz, M., Schroeder, S., Daskalakis, N., Barthel, S., Heinold, B., and Lohmann, U.: The global aerosol–climate model ECHAM6.3–HAM2.3 – Part 1: Aerosol evaluation, Geosci. Model Dev., 12, 1643–1677, https://doi.org/10.5194/gmd-12-1643-2019, 2019.

Tröstl, J., Chuang, W. K., Gordon, H., Heinritzi, M., Yan, C., Molteni, U., Ahlm, L., Frege, C., Bianchi, F., Wagner, R., Simon, M., Lehtipalo, K., Williamson, C., Craven, J. S., Duplissy, J., Adamov, A., Almeida, J., Bernhammer, A.-K., Breitenlechner, M., Brilke, S., Dias, A., Ehrhart, S., Flagan, R. C., Franchin, A., Fuchs, C., Guida, R., Gysel, M., Hansel, A., Hoyle, C. R., Jokinen, T., Junninen, H., Kangasluoma, J., Keskinen, H., Kim, J., Krapf, M., Kürten, A., Laaksonen, A., Lawler, M., Leiminger, M., Mathot, S., Möhler, O., Nieminen, T., Onnela, A., Petäjä, T., Piel, F. M., Miettinen, P., Rissanen, M. P., Rondo, L., Sarnela, N., Schobesberger, S., Sengupta, K., Sipilä, M., Smith, J. N., Steiner, G., Tomè, A., Virtanen, A., Wagner, A. C., Weingartner, E., Wimmer, D., Winkler, P. M., Ye, P., Carslaw, K. S., Curtius, J., Dommen, J., Kirkby, J., Kulmala, M., Riipinen, I., Worsnop, D. R., Donahue, N. M., and Baltensperger, U.: The role of low-volatility organic compounds in initial particle growth in the atmosphere, Nature, 533, 527–531, https://doi.org/10.1038/nature18271, 2016.

Vignati, E., Wilson, J., and Stier, P.: M7: An efficient size-resolved aerosol microphysics module for large-scale aerosol transport models, J. Geophys. Res. Atmospheres, 109, https://doi.org/10.1029/2003JD004485, 2004.

Wang, M., Chen, D., Xiao, M., Ye, Q., Stolzenburg, D., Hofbauer, V., Ye, P., Vogel, A. L., Mauldin, R. L. I., Amorim, A., Baccarini, A., Baumgartner, B., Brilke, S., Dada, L., Dias, A., Duplissy, J., Finkenzeller, H., Garmash, O., He, X.-C., Hoyle, C. R., Kim, C., Kvashnin, A., Lehtipalo, K., Fischer, L., Molteni, U., Petäjä, T., Pospisilova, V., Quéléver, L. L. J., Rissanen, M., Simon, M., Tauber, C., Tomé, A., Wagner, A. C., Weitz, L., Volkamer, R., Winkler, P. M., Kirkby, J., Worsnop, D. R., Kulmala, M., Baltensperger, U., Dommen, J., El-Haddad, I., and Donahue, N. M.: Photo-oxidation of Aromatic Hydrocarbons Produces Low-Volatility Organic Compounds, Environ. Sci. Technol., 54, 7911–7921, https://doi.org/10.1021/acs.est.0c02100, 2020.

Weisenstein, D. K., Penner, J. E., Herzog, M., and Liu, X.: Global 2-D intercomparison of sectional and modal aerosol modules, Atmospheric Chem. Phys., 7, 2339–2355, https://doi.org/10.5194/acp-7-2339-2007, 2007.

Westervelt, D. M., Pierce, J. R., Riipinen, I., Trivitayanurak, W., Hamed, A., Kulmala, M., Laaksonen, A., Decesari, S., and Adams, P. J.: Formation and growth of nucleated particles into cloud condensation nuclei: model–measurement comparison, Atmospheric Chem. Phys., 13, 7645–7663, https://doi.org/10.5194/acp-13-7645-2013, 2013.

https://doi.org/10.5194/egusphere-2026-3636
Preprint. Discussion started: 24 July 2026

Whitby, E. R. and McMurry, P. H.: Modal Aerosol Dynamics Modeling, Aerosol Sci. Technol., 27, 673–688, https://doi.org/10.1080/02786829708965504, 1997.

Williams, J., de Reus, M., Krejci, R., Fischer, H., and Ström, J.: Application of the variability-size relationship to atmospheric aerosol studies: estimating aerosol lifetimes and ages, Atmospheric Chem. Phys., 2, 133–145, https://doi.org/10.5194/acp-2-133-2002, 2002.

Wright, D. L., McGraw, R., and Rosner, D. E.: Bivariate Extension of the Quadrature Method of Moments for Modeling Simultaneous Coagulation and Sintering of Particle Populations, J. Colloid Interface Sci., 236, 242–251, https://doi.org/10.1006/jcis.2000.7409, 2001.

Wu, S., Tao, J., Ma, N., Kuang, Y., Zhang, Y., He, Y., Sun, Y., Xu, W., Hong, J., Xie, L., Wang, Q., Su, H., and Cheng, Y.: Particle number size distribution of PM1 and PM10 in fogs and implications on fog droplet evolutions, Atmos. Environ., 277, 119086, https://doi.org/10.1016/j.atmosenv.2022.119086, 2022.

Wu, Z., Liu, D., Zhao, T., Su, Y., and Zhou, B.: Size Distributions of Water-Soluble Inorganic Ions in Atmospheric Aerosols During the Meiyu Period in the Yangtze River Delta, China, Front. Environ. Sci., 9, https://doi.org/10.3389/fenvs.2021.788115, 2021.

Yan, C., Yin, R., Lu, Y., Dada, L., Yang, D., Fu, Y., Kontkanen, J., Deng, C., Garmash, O., Ruan, J., Baalbaki, R., Schervish, M., Cai, R., Bloss, M., Chan, T., Chen, T., Chen, Q., Chen, X., Chen, Y., Chu, B., Dällenbach, K., Foreback, B., He, X., Heikkinen, L., Jokinen, T., Junninen, H., Kangasluoma, J., Kokkonen, T., Kurppa, M., Lehtipalo, K., Li, H., Li, H., Li, X., Liu, Y., Ma, Q., Paasonen, P., Rantala, P., Pileci, R. E., Rusanen, A., Sarnela, N., Simonen, P., Wang, S., Wang, W., Wang, Y., Xue, M., Yang, G., Yao, L., Zhou, Y., Kujansuu, J., Petäjä, T., Nie, W., Ma, Y., Ge, M., He, H., Donahue, N. M., Worsnop, D. R., Kerminen, V.-M., Wang, L., Liu, Y., Zheng, J., Kulmala, M., Jiang, J., and Bianchi, F.: The Synergistic Role of Sulfuric Acid, Bases, and Oxidized Organics Governing New-Particle Formation in Beijing, Geophys. Res. Lett., 48, e2020GL091944, https://doi.org/10.1029/2020GL091944, 2021.

Yao, L., Garmash, O., Bianchi, F., Zheng, J., Yan, C., Kontkanen, J., Junninen, H., Mazon, S. B., Ehn, M., Paasonen, P., Sipilä, M., Wang, M., Wang, X., Xiao, S., Chen, H., Lu, Y., Zhang, B., Wang, D., Fu, Q., Geng, F., Li, L., Wang, H., Qiao, L., Yang, X., Chen, J., Kerminen, V.-M., Petäjä, T., Worsnop, D. R., Kulmala, M., and Wang, L.: Atmospheric new particle formation from sulfuric acid and amines in a Chinese megacity, Science, 361, 278–281, https://doi.org/10.1126/science.aao4839, 2018.

Young, L.-H., Lee, S.-H., Kanawade, V. P., Hsiao, T.-C., Lee, Y. L., Hwang, B.-F., Liou, Y.-J., Hsu, H.-T., and Tsai, P.-J.: New particle growth and shrinkage observed in subtropical environments, Atmospheric Chem. Phys., 13, 547–564, https://doi.org/10.5194/acp-13-547-2013, 2013.

Yu, F. and Luo, G.: Simulation of particle size distribution with a global aerosol model: contribution of nucleation to aerosol and CCN number concentrations, Atmospheric Chem. Phys., 9, 7691–7710, https://doi.org/10.5194/acp-9-7691-2009, 2009.

Yu, M. and Lin, J.: Binary homogeneous nucleation and growth of water–sulfuric acid nanoparticles using a TEMOM model, Int. J. Heat Mass Transf., 53, 635–644, https://doi.org/10.1016/j.ijheatmasstransfer.2009.10.032, 2010.

https://doi.org/10.5194/egusphere-2026-3636
Preprint. Discussion started: 24 July 2026

Yu, M., Lin, J., and Chan, T.: A New Moment Method for Solving the Coagulation Equation for Particles in Brownian Motion, Aerosol Sci. Technol., 42, 705–713, https://doi.org/10.1080/02786820802232972, 2008.

Zaveri, R. A., Easter, R. C., Fast, J. D., and Peters, L. K.: Model for Simulating Aerosol Interactions and Chemistry (MOSAIC), J. Geophys. Res. Atmospheres, 113, https://doi.org/10.1029/2007JD008782, 2008.

Zhang, D., Li, Z., Wu, H., Wu, T., Ren, R., Cai, Z., Liang, C., and Chen, L.: Analysis of aerosol particle number size distribution and source attribution at three megacities in China, Atmos. Environ., 279, 119114, https://doi.org/10.1016/j.atmosenv.2022.119114, 2022.

Zhang, K., Xu, Z., Zhang, F., and Wang, Z.: Unveiling the organic contribution to the initial particle growth in 3–10 nm size range, Atmospheric Chem. Phys., 26, 2241–2254, https://doi.org/10.5194/acp-26-2241-2026, 2026.

Zhang, R., Khalizov, A., Wang, L., Hu, M., and Xu, W.: Nucleation and Growth of Nanoparticles in the Atmosphere, Chem. Rev., 112, 1957–2011, https://doi.org/10.1021/cr2001756, 2012.

Zhang, Y., Peräkylä, O., Yan, C., Heikkinen, L., Äijälä, M., Daellenbach, K. R., Zha, Q., Riva, M., Garmash, O., Junninen, H., Paatero, P., Worsnop, D., and Ehn, M.: A novel approach for simple statistical analysis of high-resolution mass spectra, Atmospheric Meas. Tech., 12, 3761–3776, https://doi.org/10.5194/amt-12-3761-2019, 2019.

Zhang, Z., Wang, J., Riemer, N., Wang, J., Liu, C., Jin, Y., Tian, Z., Shen, S., Wang, B., Chen, G., Zhao, B., Hu, J., Wang, M., Su, H., Wang, S., Cheng, Y., and Ding, A.: The Droplet Activation Parameterization for Black Carbon-Containing Particles in Steady State, Geophys. Res. Lett., 52, e2024GL114433, https://doi.org/10.1029/2024GL114433, 2025.

Zhao, B., Donahue, N. M., Zhang, K., Mao, L., Shrivastava, M., Ma, P.-L., Shen, J., Wang, S., Sun, J., Gordon, H., Tang, S., Fast, J., Wang, M., Gao, Y., Yan, C., Singh, B., Li, Z., Huang, L., Lou, S., Lin, G., Wang, H., Jiang, J., Ding, A., Nie, W., Qi, X., Chi, X., and Wang, L.: Global variability in atmospheric new particle formation mechanisms, Nature, 631, 98–105, https://doi.org/10.1038/s41586-024-07547-1, 2024.

Zhu, Y., Shen, Y., Li, K., Meng, H., Sun, Y., Yao, X., Gao, H., Xue, L., and Wang, W.: Investigation of Particle Number Concentrations and New Particle Formation With Largely Reduced Air Pollutant Emissions at a Coastal Semi-Urban Site in Northern China, J. Geophys. Res. Atmospheres, 126, e2021JD035419, https://doi.org/10.1029/2021JD035419, 2021.